Master's Thesis

Synthesis and Application of Redox-Responsive Hyperbranched Polyglycerols

Haeree Park

Department of Chemical Engineering

Graduate School of UNIST

2018

Synthesis and Application of Redox-Responsive Hyperbranched Polyglycerols

Haeree Park

Department of Chemical Engineering

Graduate School of UNIST

Synthesis and Application of Redox-Responsive Hyperbranched Polyglycerols

A thesis/dissertation
submitted to the Graduate School of UNIST
in partial fulfillment of the
requirements for the degree of
Master of Engineering

Haeree Park

11/ 20/ 2017
Approved by

signature

Advisor: Byeong-Su Kim

Synthesis and Application of Redox-Responsive Hyperbranched Polyglycerols

Haeree Park

This certifies that the dissertation of Haeree Park is approved.

11/ 20/ 2017

signature

Advisor: Byeong-Su Kim

signature

Tae-Hyuk Kwon: Thesis Committee Member #1

signature

Ja-Hyoung Ryu: Thesis Committee Member #2

Abstract

Hyperbranched polyglycerols (*hb*PGs) are one of the most popular hyperbranched polymers. Similar to its polyether analogue, poly(ethylene glycol) (PEG), *hb*PG exhibits excellent immunogenicity and biocompatibility. Moreover, PGs have attracted significant attention as promising candidates for biomedical applications including drug delivery carriers, such as nanogels. To be specific, nanogels are actively investigated as a popular platform for advanced biomedical applications owing to their unique advantages that combine the characteristics of hydrogels and nanoparticles. For these purpose, a self-cross-linked *hb*PG nanogels are developed.

In this thesis/dissertation, we cover the subject of "Synthesis of Redox-Responsive Hyperbranched Polyglycerols and Their Applications". First of all, the overview of the *hb*PG research and stimuli-responsive nanogel is given in part 1. After that, researches on "Redox-degradable *hb*PG and their degradation" and "Reduction triggered self-cross-linked *hb*PG nanogel" will be presented in part 2 and 3, respectively.

Contents

List of Figures

time (Table 2); d) NaN_3, DMF, 60 °C, 24 h; e) propargyl derivative, $CuSO_4 \cdot 5H_2O$, sodium ascorbate, H_2O, 24 h.

Figure 8. Scheme for synthesis of nanogel by emulsion polymerization a) with emulsion, b) without emulsion c) cross-linking of amphiphilic block copolymer in shell or core of the micelles in water.

Figure 9. (a) Images of disulfide containing hyperbranched polymer crosslinking after heating and in un-crosslinked state on keeping at low temperature. (b) Chemical structure and illustration of a light-sensitive cholesteryl pullulan nanogel. (c) The effect of structural variations in acetal- and ketal-based linkers upon their degradation kinetics (d) Illustration of in situ forming reduction-sensitive nanogels for facile loading and triggered release of proteins.

Figure 10. (a) Scheme for the preparation of biodegradable nanogels with surface modification. (b) Scheme for the synthesis of size-controllable PSSG nanogels with different amounts of DTT. (c) Selective release of hydrophobic and hydrophilic therapeutics from various responsive nanogels upon different stimuli.

Figure 11. (a) Nanogel-cross-linked thin films for adhesion proteins and cytokines (b) Preparation of NRP+I and schematic illustration of chemo-immunotherapy. (c) Schematic illustration of CXCR4-targeted Dox delivery by bio-reducible dextrin nanogel in metastatic breast cancer.

[Part 2]

Figure 1. Synthetic pathway and degradation structure of two types of redox-degradable hyperbranched block copolymers; (a) shell-degradable P(G-*b*-SSG) and (b) core-degradable P(SSG-*b*-G).

Figure 2. ^{1}H NMR spectra before and after addition of the second monomer to confirm the successful synthesis of the hyperbranched block copolymers of (a) P(G_{130}-*b*-SSG_{80}) and (b) P(SSG_{30}-*b*-G_{100}).

Figure 3. DSC curves for PG_{130} (blue), P(G_{130}-*b*-SSG_{80}) (sky blue), P(SSG_{30}-*b*-G_{100}) (yellow), $PSSG_{30}$ (red), and a simple blend of PG_{150} and $PSSG_{50}$ homopolymers (green). Star marks indicate the glass transition temperatures (T_g) for each polymer.

Figure 4. Schematic degradation structure of PSSG polymers and the corresponding GPC traces of (a) P(G_{130}-*b*-SSG_{80}), (b) $PSSG_{30}$, (c) P(SSG_{30}-*b*-G_{50}), and (d) P(SSG_{30}-*b*-G_{100}) before (black curve) and after (red curve) degradation.

Figure 5. ^{1}H NMR spectra of $PSSG_{30}$ homopolymer and detailed assignments of the respective protons giving rise to these signals.

Figure 6. *In vitro* cell viability assays of $PSSG_{30}$ (black), P(SSG_{30}-*b*-G_{50}) (dark grey), P(SSG_{30}-*b*-G_{100}) (grey), and P(G_{130}-*b*-SSG_{80}) (white) polymers determined by MTT assay using (a) WI-38 (normal cell) and (b) HeLa (cancer cell).

[Part 3]

Figure 1. Synthetic scheme for the PSSG polymer and *in situ* formation of degradable nanogels through thiol–disulfide exchange and disulfide exchange chemistry (marked with blue arrows) between inter- and intra-molecular chains upon treatment with DTT. Other chains are not depicted for clarity. Green circle represents the basic unit for the formation of the PSSG nanogel.

Figure 2. (a) Scheme for the synthesis of size-controllable PSSG nanogels with different amounts of DTT. (b) Representative AFM images of nanogels (NGs) prepared from $PSSG_{30}$ homopolymer (polymer 2) and P(G_{10}-*co*-SSG_{12}) copolymer (polymer 3) with 10 and 50 mol % of DTT.

Figure 3. Hydrodynamic diameter (D_h) of NGs prepared from P(G_{10}-*co*-SSG_{12}) copolymer (polymer 3) with varying degrees of DTT treatment. Note that the D_h of the initial P(G_{10}-*co*-SSG_{12}) copolymer (green) is determined to be only 2 nm.

Figure 4. Release profile of Nile red from NGs with different cross-linking densities. Note that

the shaded time points represent treatment of the Nile red-loaded NGs with additional DTT for an active delivery mode.

Figure 5. (a) *In vitro* cell viability assay of plain NG4 (black) and Dox-loaded NG4 (red). (b) CLSM images of HeLa cells incubated with Dox-loaded NG4 for 6 h (top panel) and 24 h (bottom panel). Each channel corresponds to the fluorescence of DAPI for cell nucleus and Dox for drug delivery. Scale bar is 20 μm.

Figure 6. (a) CLSM images of HeLa cells incubated with NG4 loaded with both Dox and the FITC-labeled β-galactosidase (FITC-β-gal). Each channel corresponds to the red color of Dox, the green for FITC-β-gal, and the blue Hoechst stain in the cell nucleus. (b) X-gal activity assay of delivered β-gal into HeLa cells using NG4. Control samples of free cells and β-gal only. Note that the free cells indicate the X-gal activity due to the presence of internal β-gal in the lysosome. Scale bar is 10 μm.

List of Schemes

List of Tables

Part 1. Introduction of Hyperbranched polyglycerol and biodegradable nanogels

1. Hyperbranched polyglycerol

Hyperbranched polymer is a kind of dendritic macromolecules with random branch-on-branch topology.[1] This polymer has a densely branched structure and a number of terminal groups. Hyperbranched polyglycerol can be accessible in a one-step synthesis via ring-opening multi-branching polymerization (ROMBP) of glycidol which is extremely reactive epoxide under slow monomer addition (SMA) reaction. Based on the SMA method, Frey group succeeded the polymerization of the glycidol in 1999.[2-4] A schematic illustration of hyperbranched polyglycerol is shown in Figure 1.[5] Moreover, functional core can be easily changed and hydroxyl group can be modified into various types of polymers by introducing new multihydroxy-functional group.

Hyperbranched polyglycerols with controlled molecular weights have been prepared via anionic polymerization of glycidol with rapid cation-exchange equilibrium. Furthermore, it allows them to prevent broad molecular-weight distribution of random AB_m-type polycondensation. Brooks and co-workers observed the formation PG which has a high molecular weight with very narrow dispersion using dioxane in 2006.[6] The method can provide PG with high molecular weight which is significant for various applications. Synthetic process is followed by initiator formation, initiation/propagation, intramolecular transfer and intermolecular transfer as shown in Figure 2.[5] In this procedure, glycidol is slowly added into the solution which contained trifunctional core-initiator. During the polymerization, the primary and secondary alcohols chain ends can grow at the same time, resulting in a branched structure due to the extremely fast proton exchange.

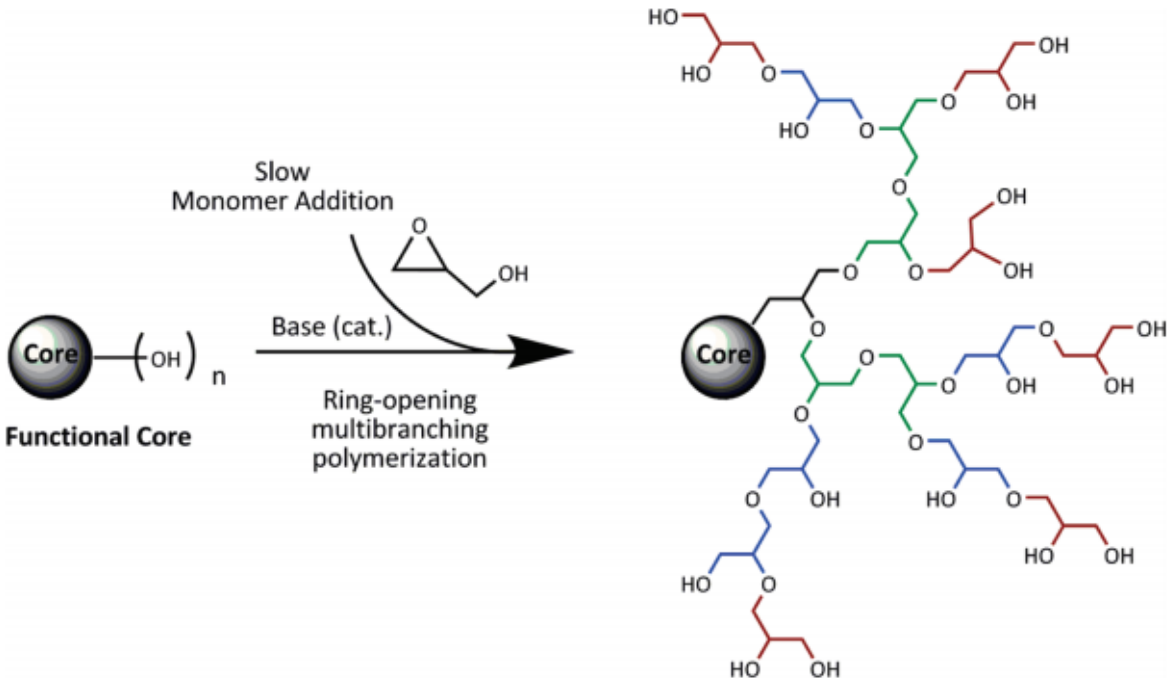

Figure 1. Scheme for hyperbranched polyglycerols synthesis using anionic ring-opening polymerization. Reprinted with permission from *Acc. Chem. Res.* **2010**, *43*, 129–141. Copyright 2010 American Chemical Society.

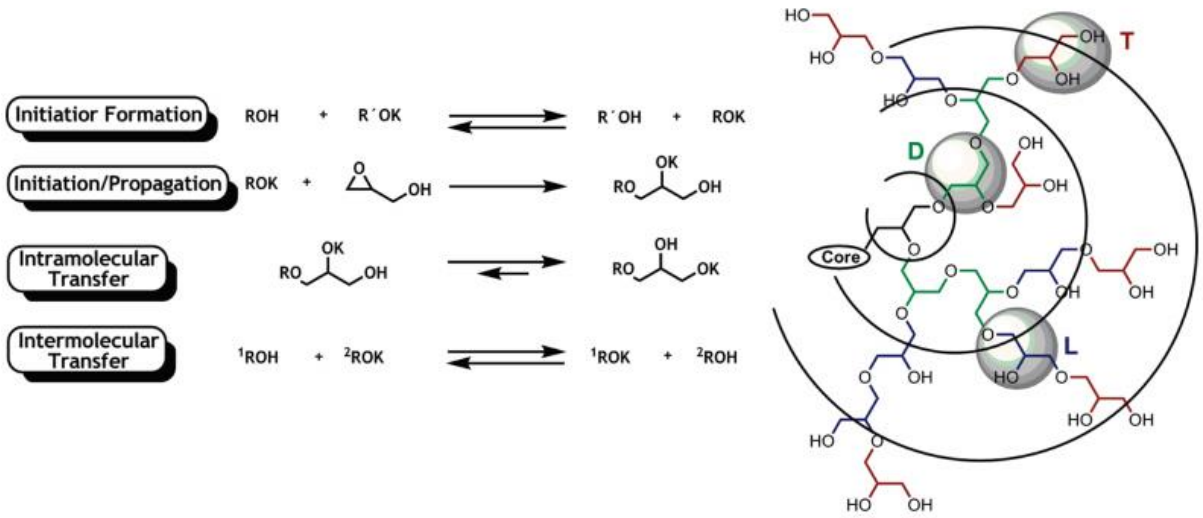

Figure 2. Synthetic pathway of hyperbranched polyglycerol via base-catalyzed ring-opening polymerization using glycidol. branched ("dendritic", D) units, linear units (L), and end groups ("terminal units", T). Reprinted with permission from *Acc. Chem. Res.* **2010**, *43*, 129–141. Copyright 2010 American Chemical Society.

2. Polyglycerol with various polymer architectures and functionalities

The overview in Figure 3 shows the versatile synthetic strategy of PG or polyether polyol and the other functional epoxide comonomers.[7] The first site (I) which can be modulated is initiator as various functional molecules. The second site (II) is enormous kind of epoxide monomers can be easily tuned with various molecules and polymerized in a block or random manner. The third site (III) which is further modification of the polyether polyol or PG resulting in new functions and properties. After all, it can be applied in many fields such as biomedical application, support for catalysts, and polymer electrolyte. These three sites will be covered below.

The synthesis of hyperbranched polyglycerol with various functional core units and modification of epoxide monomer is an important approach because it leads to gain the specific properties of PGs such as solubility, particle size, biocompatibility and fluorescent probe. The core initiator must have hydroxyl group for initiation reaction and suitable initiator should be used to maintain strict oxyanionic polymerization condition. Moreover, there are various synthetic methods to adjust the hydroxyl group of the PG backbone. The hydroxyl groups can be ornamented in a variety of functional groups. In recent years, there are some development to decorate initiator and monomer for functional PGs.[8-10]

Haag group developed a new method for the cationic polymerization of glycidol by citric acid at natural and solvent-free conditions.[11] Citric acid is a proton donor and can be contained in the structure of polyglycerol by reaction with the activated monomer. Organic solvents or other reagents have not been used in the synthetic processes aside from citric acid, glycidol, and water. Taking advantage of the green synthesis, biocompatibility of polyglycerol and ability to use the polyglycerol with citric acid is a promising candidate in biomedical application fields in Figure 4a.

In 2011, Haag group also reported synthesis of polyanionic molecules according to hyperbranched polyglycerol.[12] Moreover, the synthesis of dendritic polyglycerol was performed through a direct hydroxyl group interconversion. The order of efficiency of L-selectin inhibition is followed by carboxylate < phosphate < phosphonate ≈ sulfonate < bisphosphonate < sulfate in Figure 4b.

In 2014, Jana group reported surface modification approach for fluorescent silicon nanoparticle.[13] This nanoparticle can transform hydrophobic nanoparticle into water-soluble nanoparticle of high colloidal stability. They conducted a ring-opening polymerization of

glycidol at the hydroxyl-terminated nanoparticle surface, then results in hyperbranched polyglycerol grafted silicon nanoparticle. This silicon nanoparticle-based fluorescent probe can be used for *in vitro/in vivo* bioimaging applications in Figure 4c.

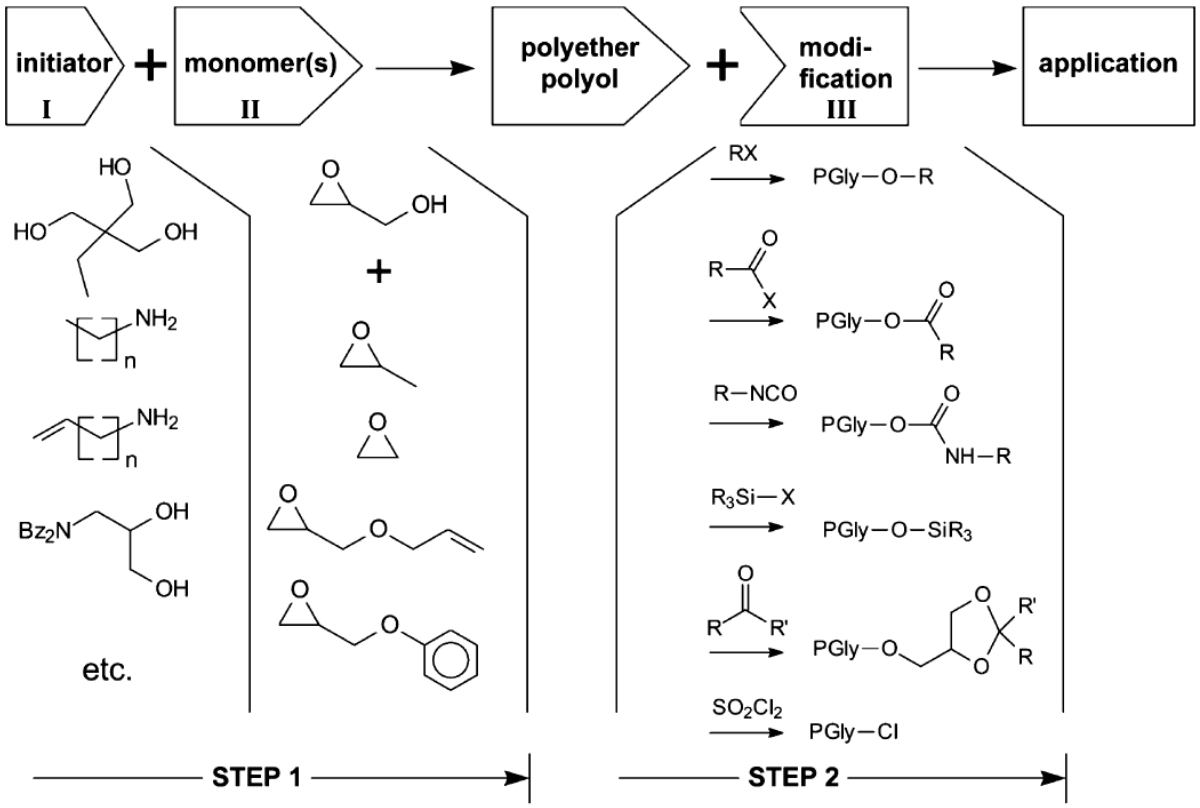

Figure 3. Modular system for the synthesis of hyperbranched polyether polyols and respective derivatives. Reprinted with permission from *Mol. Biotechnol.* **2002**, *90*, 257–267. Copyright 2002 Springer.

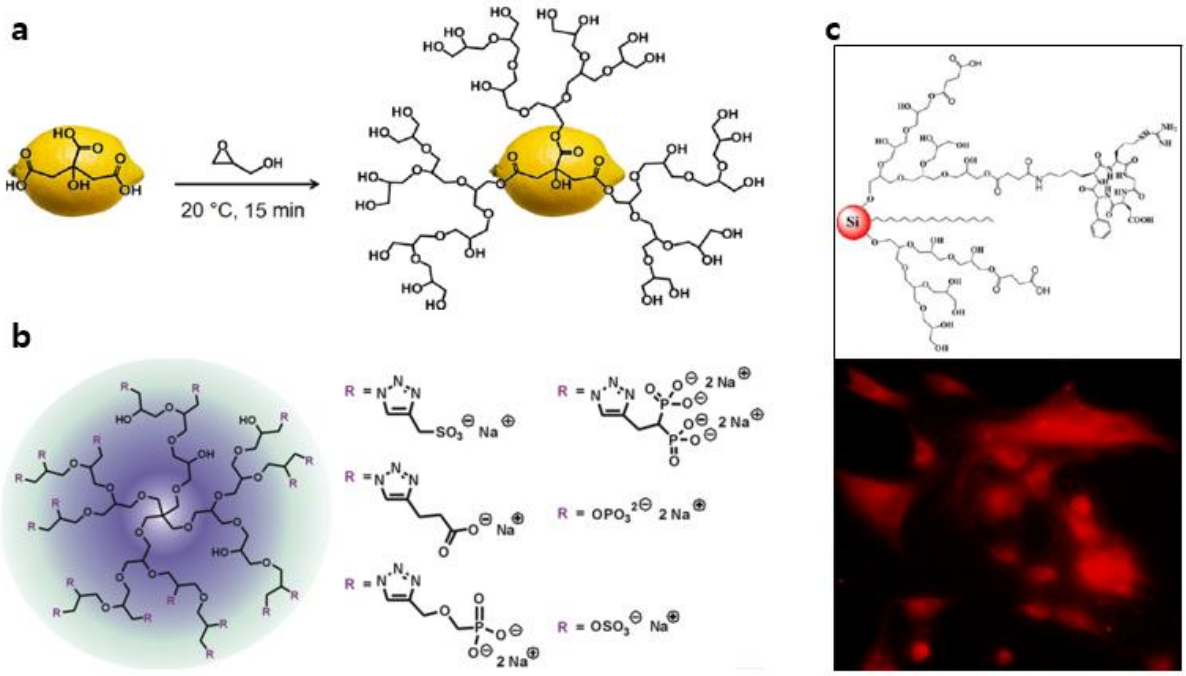

Figure 4. PGs with (a) citric acid initiator, (b) alkyne-functionalized anions such as sulfonates, carboxylates, phosphonates, and bisphosphonates, (c) silicon nanoparticles as single focal group for green synthesis, synthesis of dendritic polyglycerol, and bioimaging probe, respectively. Reprinted with permission from (a) *ACS Macro Lett.* **2017**, *6*, 35–40, (b) *Biomacromolecules* **2011**, *12*, 2502–2511, (c) *ACS Appl. Mater. Interfaces* **2014**, *6*, 4301–4309. Copyright 2011, 2014, 2017 American Chemical Society.

2.1. Redox-active polymer

Stimuli-degradable PGs and its monomer are recently developed by many research groups. Especially, redox-responsive polymer has recently emerged as an important area. For example, disulfide or ferrocene functionalities as a redox sensitive linkage can be attached to epoxy monomer for synthesizing redox-responsive polymer. As the advantages of using redox sensitive linkage into carriers, it can trigger cellular delivery applications by means of glutathione (GSH), one of the main reducing agents inside cells and the most abundant in the cytosol. In 2011, Yan group reported that novel redox-responsive polyphosphate nanosized assemblies based on amphiphilic hyperbranched multiarm copolyphosphates with backbone redox-responsive, good biocompatibility, and biodegradability simultaneously have been synthesized successfully. This micellar structure can be disassembled in response to reducing agent and result in a released therapeutic.[14] Moreover, disulfide-linked amphiphilic polymer-docetaxel conjugates assembled redox-sensitive micelles for efficient antitumor drug delivery are reported in 2016.[15] Copolymers with different molecular weight (mPEG2000-PBLG1750 and mPEG5000-PBLG1750) were synthesized via the ring opening polymerization (ROP) initiated by monoamino-terminated mPEG (mPEG-NH_2). Then, the docetaxel (DTX) was conjugated to the block polymers through a linkage containing disulfide bond to obtain mPEG-PBLGSS- DTXs. The obtained copolymer-drug conjugates mPEG2000-PBLG1750-SS-DTX could self-assemble into nanosized micelles in aqueous environment with a low critical micelle concentration (CMC, 3.98 μg/mL). Xia group also introduced redox-degradable hydrogels with controllable tunable mechanical properties.[16] This hydrogel composed of recombinant silk-elastin-like protein polymers were synthesized with various ratio of silk-to-elastin blocks. These polymers also contained redox-sensitive linkage of a highly polar model drug from the hydrogels *in vitro*. The resulting hydrogels with tunable mechanical properties and redox-sensitive features may be potentially useful as biomaterials with various applications such as drug delivery and tissue engineering. Huang group introduced self-assembly of homopolymers containing carboxyl functionalities and ferrocene in 2013.[17] Three new acrylamide monomer composed tert-butyl ester groups and ferrocene were prepared through multistep nucleophilic substitution reaction followed by reversible addition−fragmentation chain transfer (RAFT) homopolymerization. Large compound micelles from amphiphilic homopolymers were formed with different morphologies.

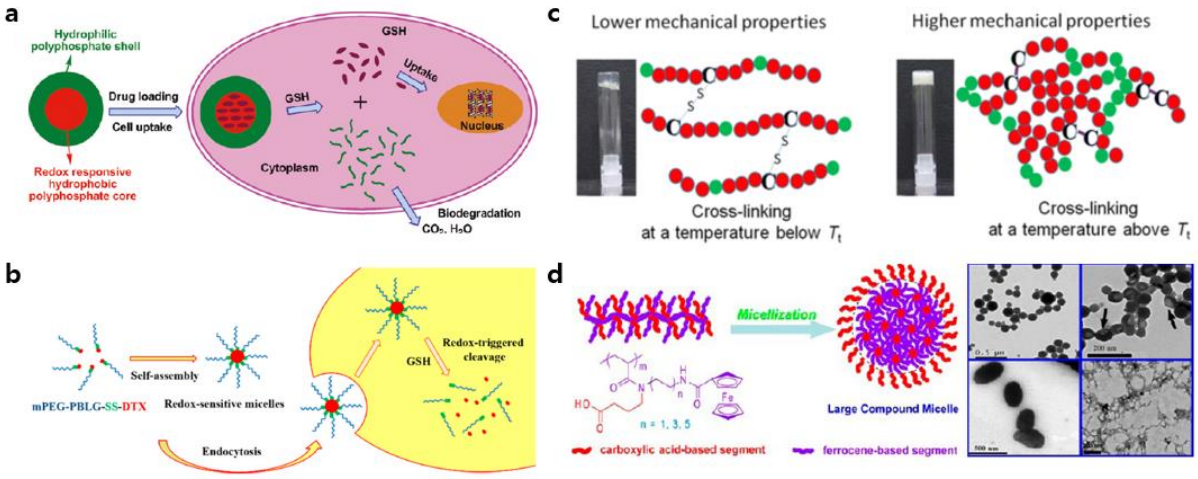

Figure 5. (a) Redox-sensitive polyphosphate micelles delivered drugs into the nuclei of tumor cells. (b) Schematic diagram of mPEG-PBLG-SS-DTXs micelles self-assembly, endocytosis by tumor cells, as well as the redox-triggered drug release. (c) Rationally designed redox-sensitive protein hydrogels with tunable mechanical properties. (d) Synthesis of self-assembly micelles using ferrocene-containing amphiphilic homopolymers. Reprinted with permission from (a) *Biomacromolecules* **2011**, *12*, 2407–2415, (b) *Biomacromolecules* **2016**, *17*, 1621–1632, (c) *Biomacromolecules* **2016**, *17*, 3508–3515, (d) *Langmuir* **2013**, *29*, 10922–10931. Copyright 2011, 2013, 2016 American Chemical Society.

3. Applications of hyperbranched PG

3.1. Biomedical applications

The best motivation of the significant interest to PGs is various synthetic routes to their derivatives and their excellent biocompatibility. Brooks groups demonstrate that biocompatibility testing of hyperbranched PGs conducted *in vitro* as well as in vivo.[18] Results from these studies show that PGs are not only highly biocompatible but also were found to be well tolerated by mice even when injected in high doses. From this study, *hb*PG and their derivatives could attract increasing interests for drug-delivery, macromolecular therapeutics, and other biomedical applications. Moreover, *hb*PG is very promising candidate as drug delivery carrier due to its many hydroxyl groups, which can give many possibilities for modification with other functional groups and biomolecules. Frey group also introduce major potential field of PG for biomedical application such as human serum albumin substitute, and alternatives to heparin as an injectable anticoagulant (Figure 6a).[19] To be more specific, Frey group also synthesize and noncovalently conjugate avidin with 2-(4-hydroxyphenylazo)benzoic acid (Figure 6b).[20] In 2012, our group report polyglycerol system conjugated anti-cancer drug for drug delivery (Figure 6c).[21] To be more specific, we synthesized well-defined hyperbranched double hydrophilic block copolymer of poly-(ethylene oxide)-hyperbranched-polyglycerol (PEO-*hb*-PG) to progress an efficient drug delivery system. This polymer demonstrates the efficient conjugation of hydrophobic doxorubicin and enhancement of targeting capacity to the tumor cell. In addition, we confirmed the rapid release of doxorubicin via the cleavage of hydrazone bonds under the acidic condition and its significant cytotoxicity to cancer cell. In 2017, Haag group investigated solution behavior, encapsulation and release properties, biocompatibility, and cellular uptake pathways of fullerene-polyglycerol amphiphiles with defined structures.[22] Owing to their unique properties and structure, water-soluble fullerene derivatives are of great interest for various biomedical applications. Conjugation of a pH-sensitive dye to the fullerene-polyglycerol amphiphiles as a probe showed that their self-assemblies are taken up through endocytotic pathways. Release of encapsulated hydrophobic dyes from fullerene-polyglycerol amphiphiles strongly depends on the number of their branches. Taking advantage of fullerene-polyglycerol amphiphiles, such as water solubility, biocompatibility, and transfer-ability, it might be used as unimolecular carriers for future biomedical purposes (Figure 6d).

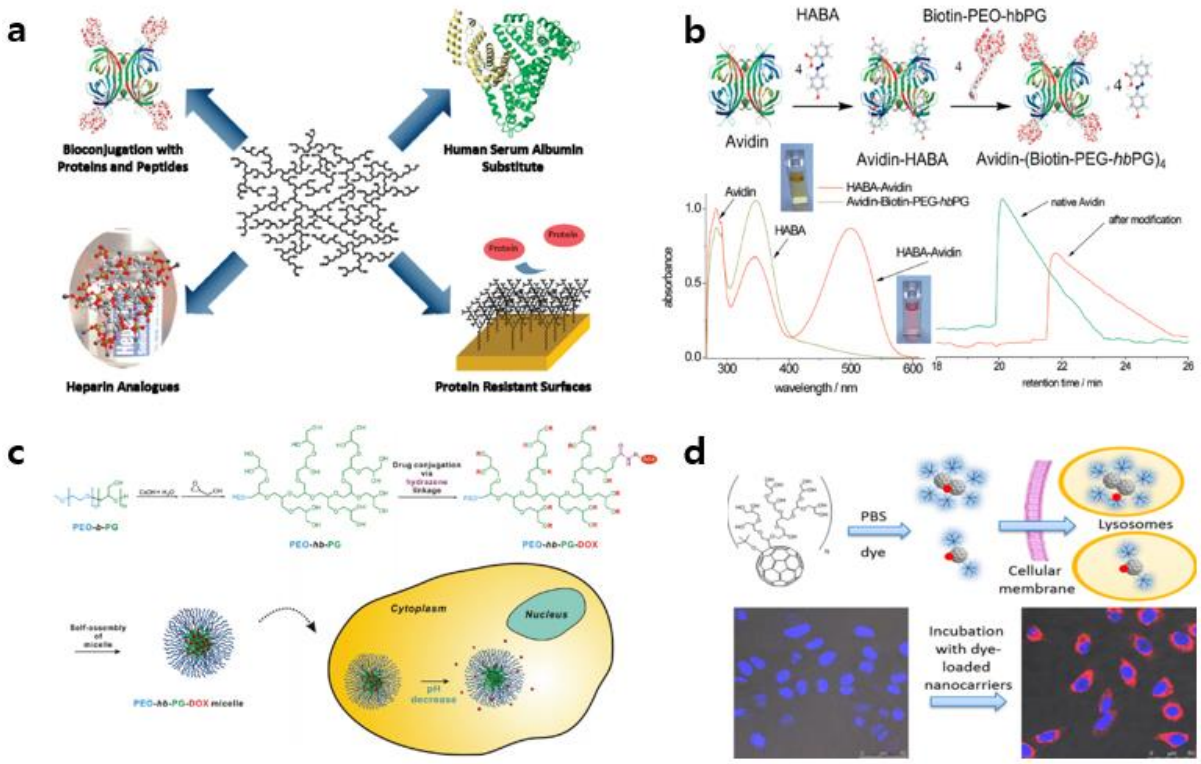

Figure 6. (a) Scheme for biomedical application areas revealed for *hb*PG. (b) Scheme of conjugation avidin with 2-(4-hydroxyphenylazo)benzoic acid and Check the amount of avidin using UV. (c) Illustration of drug-polymer conjugate of doxorubicin conjugated poly(ethylene oxide)-*hb*-PG and its self-assembled micelle formation for the pH-responsive intracellular release of anti-cancer drug. (d) Fullerene polyglycerol amphiphiles as unimolecular transporters. Reprinted with permission from (a) *Acc. Chem. Res.* **2010**, *43*, 129–141, (b) *J. Am. Chem. Soc.* **2009**, *131*, 7954–7955, (c) *Biomacromolecules* **2012**, *13*, 1190–1196, (d) *Langmuir* **2017**, *33*, 6595–6600. Copyright 2009, 2010, 2012, 2017 American Chemical Society.

4. Definition and synthetic method of nanogel

Nanogels are nano-sized hydrogels with three dimensional structures of polymer. In general, cured nanogels are chemically obtained under dilute conditions with cross-linking reaction of hydrophilic polymers which are altered with various function like thiol and vinyl groups. Moreover, nanogels are actively developed as promising platforms for advanced biomedical applications due to the unique advantages that combine the characteristics of hydrogels and nanoparticles.[23-25] Nanogel can be synthesized with fuctionalized *hb*PG, so they developed a simple method to synthesize nanogels with polyglycerol composition based upon acid-catalyzed polyaddition of commercially available starting materials such as the triol glycerol (1), and the trisepoxide, glycidyl glycerolether (2) (Figure 7).[26] This size of nanogel can be controlled around 25~350 nm.

Nanogels can be synthesized and polymerized in the core of oil-in-water (O/W) nano or microemulsion. To synthesize nanogels having well-defined bulk, microemulsion polymerization approaches has been generally utilized (Figure 8a).[27] Inverse microemulsion polymerization with water-in-oil (W/O) emulsions has lately received enormous interest (Figure 8b). Moreover, hydrophilic therapeutics such as enzymes or anticancer drugs were easily encapsulated into nanogels using these methods. Stable nanogels having narrow size distribution can be also synthesized by self-cross-linking of the hydrophobic/hydrophilic polymer network within the core or shell (Figure 8c). Moreover, chemical self-cross-linking methods have been recently advanced, for example, nanogels which is redox-responsive can be synthesized through disulfide-thiol exchange and new disulfide bonds formation as crosslinking sites. More recently, star-like nanogels were introduced, and dynamic covalent bond exchange reactions can occur for cross-linking of the core between two different block copolymers.

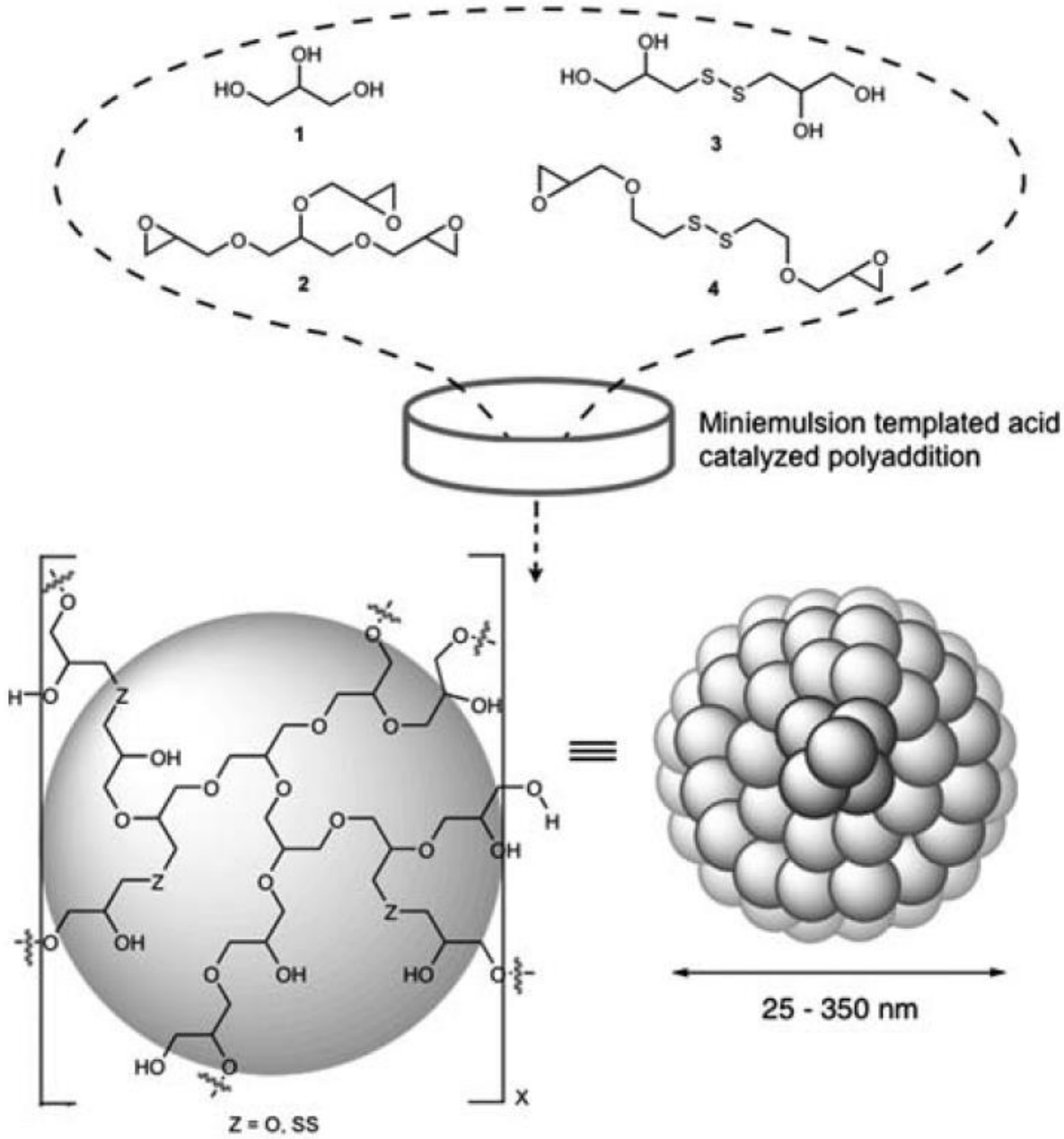

Figure 7. Polyol and polyepoxide monomers used in the miniemulsion polyaddition preparation of polyglycerol nanogel derivatives with the general structure are shown. Reprinted with permission from *Soft Matter* **2010**, *6*, 4968–4975. Copyright 2010 Royal Society of Chemistry.

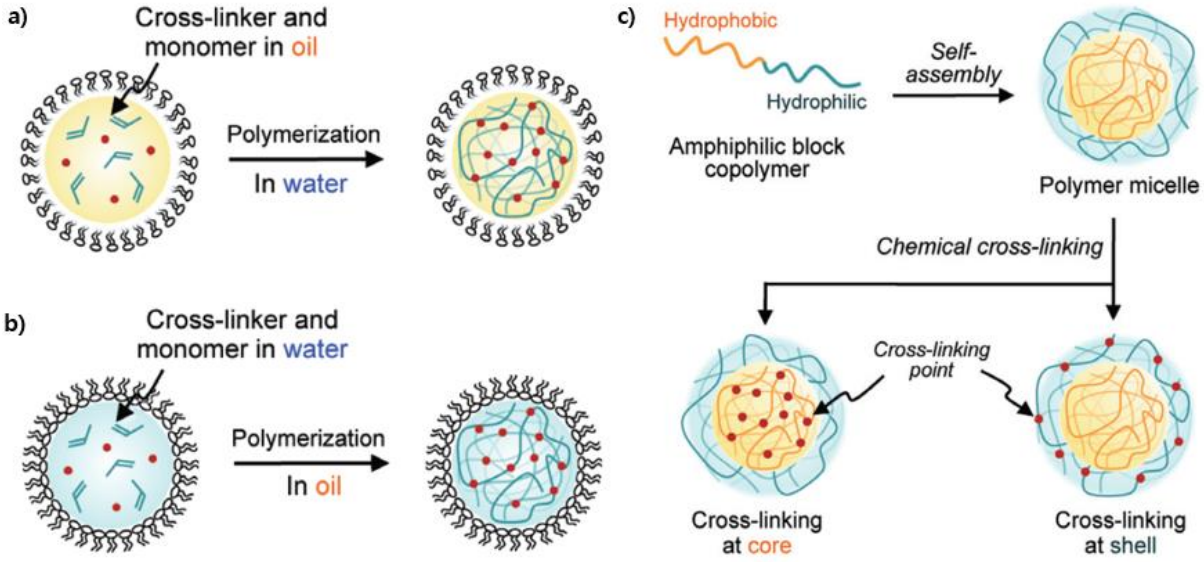

Figure 8. Scheme for synthesis of nanogel by emulsion polymerization. a) with emulsion, b) without emulsion and c) cross-linking of amphiphilic block copolymer in shell or core of the micelles in water. Reprinted with permission from *Chem. Rec.* **2010**, *10*, 366–376. Copyright 2010 Wiley Online Library.

5. Self-cross-linked nanogels

5.1. Various stimuli – temperature, light, pH and redox

Micro- and nanogels can be assembled or disassembled under biological and external stimuli, such as temperature, light, pH, and redox. There are several strategies to synthesize micro- and nanogels with crosslinking reaction.[24]

First of all, covalent crosslinking can be easily occurred when synthesizing nanogel through various processes such as radical polymerization, click chemistry (thiol-ene, michael addition, copper-free), thiol-disulfide exchange reaction, photo-induced crosslinking, and enzyme-catalyzed crosslinking. Secondly, supramolecular crosslinking can form self-assembly based on diverse physical interactions, such as hydrogen bonding, hydrophobic and ionic interaction. Supramolecular crosslinking does not require any crosslinker during the encapsulation of drug unlike the covalent crosslinking approach.

Moreover, nanogels are assembled or disassembled with cleavable covalent crosslinking, for example, acid-cleavable, redox cleavable, photo cleavable, enzyme cleavable, reversible click reaction, and additive cleavable. Moreover, the stable structure of crosslinked nanogels is cleaved under specific condition. To date, there are many papers related to these several strategies to synthesize micro- and nanogels. In 2012, Hong group reported that bio-reducible nano, and microgels synthesized through temperature-responsive condition and self-crosslinking poly(amidoamine) has been synthesized via michael addition reaction, and this is hyperbranched structure containing disulfide bonds.[28] This hyperbranched polymer cannot be dissolved in methanol for 72 h and does not dissolves in methanol at 45 °C for 100 min, indicating that this polymer can be changed with self-crosslinking upon heating as shown in Figure 9a.

A self-assembled nanogel under light-sensitive cholesteryl pullulan by using photo-labile units is introduced in Figure 9b.[29] The film nanogel can be obtained through evaporation of nanogel solution. The fabrication of patterned nanogel-based materials is introduced by a light-sensitive nanogel by cholesterol decorated with an ortho-nitrobenzyl unit on the hydroxyl group of pullulans. These approaches facilitate the polymer to release cholesteryl groups with light-responsive cleavage of the nitrobenzyl unit.

Thayumanavan group reported recently that the effect of structural variations in acetal- and ketal-based linkers through degradation kinetics with various design, synthesis, and study of six series of molecules in Figure 9c.[30] They also show that the structural fine-tuning of the

different linkers permits access to variations in kinetics of degradation through the systematic study. Following this, they studied the degradation kinetics study of polymeric nanogels that contains acetal or ketal moieties as cross-linking functionalities under pH-responsive variations.

In 2013, reduction-sensitive degradable nanogels were synthesized based block copolymers for high loading capacity in Figure 9d.[31] These copolymers were synthesized through ring-opening polymerization with cyclic carbonate groups for controllable disulfide-cross-linked nanogels around 100 nm. The nanogel sizes decreased as increasing acryloyl carbonate units, followed by increased cross-linking density. Moreover, Fluorescein(FITC)-labeled cytochrome C could be encapsulated into nanogels with high loading capacities.

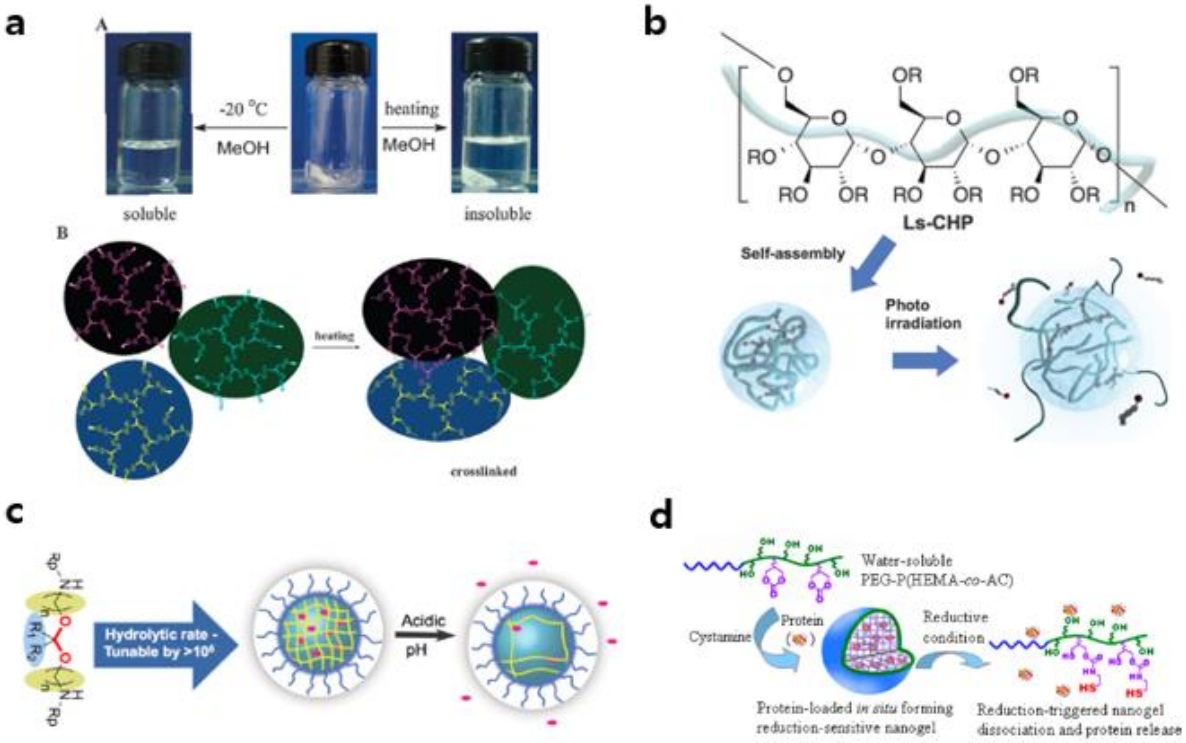

Figure 9. (a) A photograph of hyperbranched polymer which contains disulfide group crosslinked after heating and in uncrosslinked state at low temperature. (b) Illustration of a light-sensitive cholesteryl pullulan nanogel and chemical structure. (c) The effect of structural variations in acetal- and ketal-based linkers upon their degradation kinetics. (d) Illustration of in situ forming reduction-sensitive nanogels for facile loading and triggered release of proteins. Reprinted with permission from (a) *Chem. Commun.* **2012**, *48*, 5623–5625, (b) *Chem. Commun.* **2015**, *52*, 1222–1225, (c) *J. Am. Chem. Soc.* **2017**, *139*, 2306–2317, (d) *Biomacromolecules* **2013**, *14*, 1214–1222. Copyright 2012, 2013, 2015, 2017 American Chemical Society.

5.2. Control variations – size, surface functionality, hydrophilic/hydrophobic balance, and drug loading capacity

To develop the nanogel in drug delivery system, it is challenging to control precise properties such as size, surface functionality, hydrophilic/hydrophobic balance, and drug loading capacity.

It is important to control the size, cargo loading capacity, and acquire new stimuli condition by decorating the surface of the nanogel.[24] Thayumanavan group recently reported that surface-modified polymeric nanogels with drug encapsulation abilities.[32] They targeted a disulfide bond which can be susceptible to reducing like glutathione (GSH) for functionalization of particle surface. These polymer nanoparticles demonstrated by confirming that therapeutics can be noncovalently conjugated into nanoparticles, the incorporated therapeutic drug can be released under biologically relevant stimulus (Figure 10a). Nanogel exhibited enhanced permeability and retention (EPR) effect by regulating the size. It is such important that nanogel can enter tumor cells nearby. Our group recently reported the nanogel which can be tunable in size and cross-linking density depending on the type of polymer (homo- or copolymer) and the amount of reducing agent, dithiothreitol, used in the preparation of the nanogels.[33] This self-cross-linking *hb*PG nanogel could be synthesized by using the thiol-disulfide exchange reaction based on PSSG (disulfide-containing polymer) (Figure 10b). Moreover, Wang group reported hydrophilic and hydrophobic cargo from nanogel can be released in response to multi-stimuli-responsive conditions, such temperature, pH, redox and UV light. The water-soluble therapeutics were crosslinked to the nanogel with poly(dimethylaminoethyl methacrylate) (PDMAEMA) via redox degradable of disulfide bond, while hydrophobic therapeutics were noncovalently encapsulated into nanogels. For these dual-encapsulated nanogels, the water-soluble therapeutics can be released in response to reducing agent, while hydrophobic therapeutics can be released by UV light, pH, and temperature conditions (Figure 10c).[34]

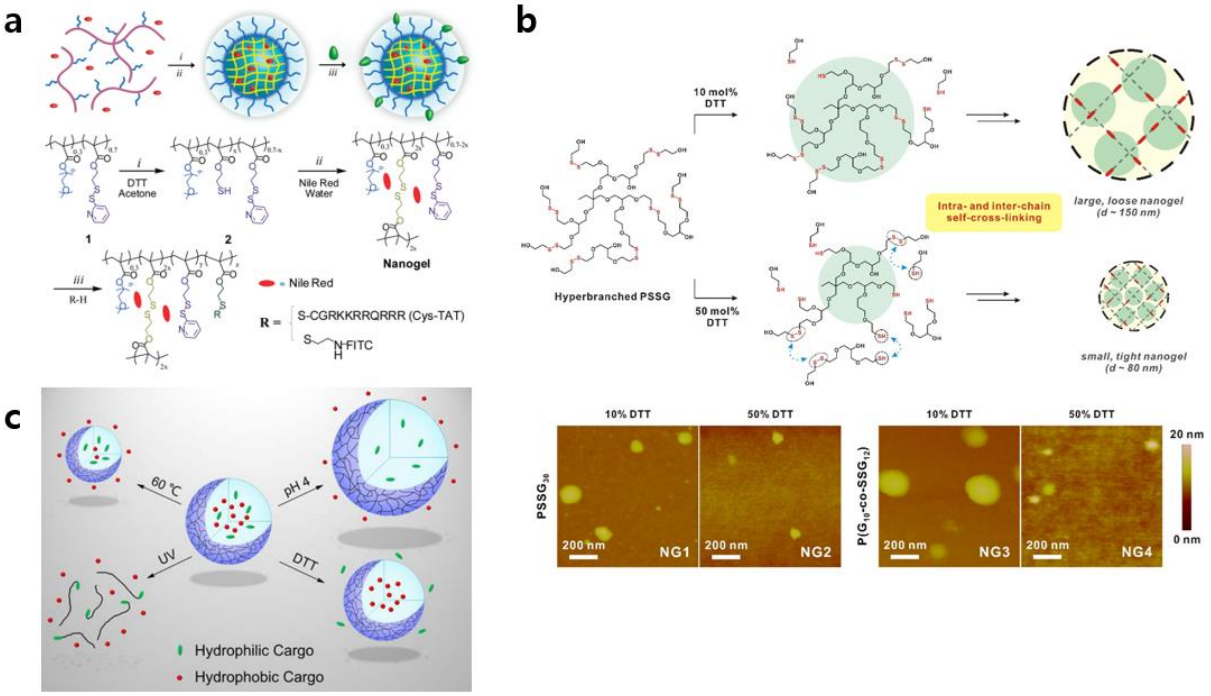

Figure 10. (a) Scheme for the preparation of biodegradable nanogels with surface modification. (b) Scheme for the synthesis of size-controllable PSSG nanogels with different amounts of DTT. (c) Selective release of hydrophobic and hydrophilic therapeutics from various responsive nanogels upon different stimuli. Reprinted with permission from (a) *J. Am. Chem. Soc.* **2010**, *132*, 8246–8247, (c) *ACS Appl. Mater. Interfaces* **2016**, *8*, 28888–28896. Copyright 2010, 2016 American Chemical Society.

6. Applications of nanogels

6.1. Biomedical application

Nanogels have been mostly used as one of the most promising biomedical application platforms due to the various advantages that have characteristics of nanoparticles and hydrogels together.[35-37] The ability to respond to external stimuli such as temperature, redox, light, pH and so forth, are most attractive in area of drug delivery system. Moreover, multi-functionalized nanogels having specificity and sensitivity were made for biomedical applications. As a result, biodegradable nanogels are anticipated to serve as smart nanocarriers and diagnostic agents for diseases in the future.

Many scientists have been working on biomedical applications of nanogels these days. In 2016, extracellular matrices from amphiphilic nanogel-cross-linked thin films to anchor adhesion enzymes are reported.[38] To be specific, novel nanogel-cross-linked film constituted of acryloyl-decorated cholesterol-containing pullulan nanogels is synthesized by Michael addition reaction. The elastic property of the films can be controlled by changing the concentration of cross-linker. The nanogels in the films induce this absorption by loading proteins and acting as anchoring. As a result, NanoClik films enables to load biological proteins as artificial matrix (Figure 11a). Moreover, tumor microenvironment responsive nanogel for the combinatorial antitumor effect of chemotherapy and immunotherapy are recently reported in Zhang group.[39] A nanogel having similar tumor microenvironment is synthesized for the effects of immunotherapy and chemotherapy. Nanogels which contain hydroxypropyl-β-cyclodextrin acrylate, positive and negative chitosan derivatives for encapsulating anticancer drug could be controlled depending on the pH condition (Figure 11b). Furthermore, in 2017, Sun group reported CXCR4-targeted and redox responsive dextrin nanogel for metastatic breast cancer therapy.[40] In this study, bioreducible crosslinked dextrin nanogel (DNG) was synthesize for various functions, such as inhibition of tumor metastasis, CXCR4 chemokine targeting, and reduction-responsive intracellular release of doxorubicin (DOX). DOX-AMD-DNG also displayed superior anticancer activity and antimetastatic effects in vivo test. In conclusion, the multifunctional DOX-AMD-DNG can effectively enter the tumor site and simultaneously hinder cancer metastasis and progression (Figure 11c).

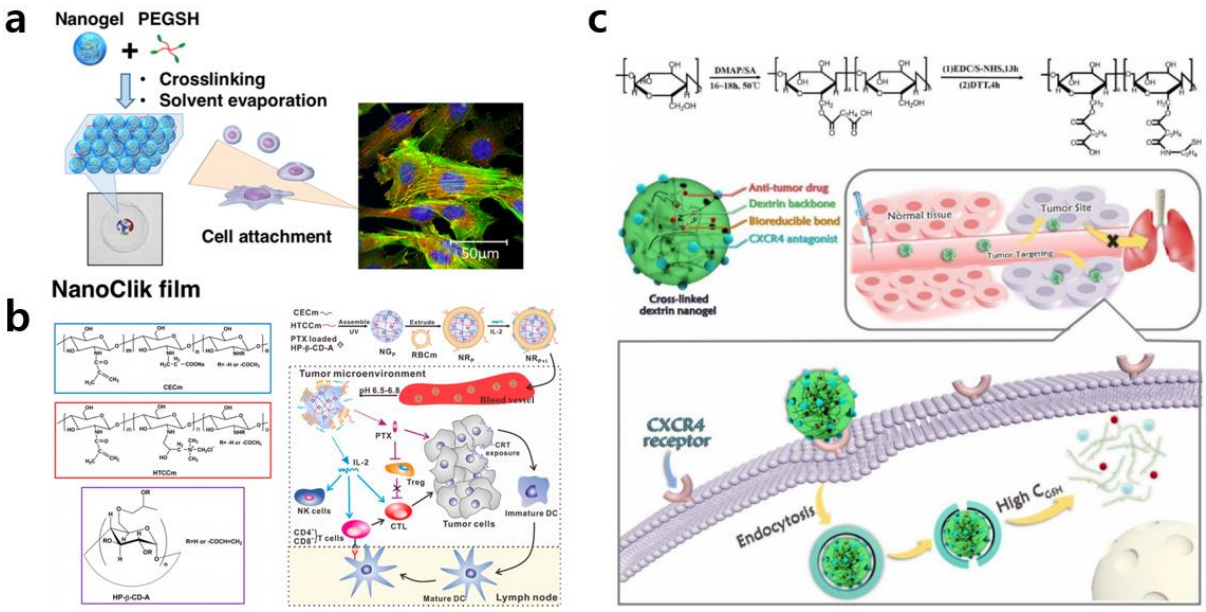

Figure 11. (a) Nanogel-cross-linked thin films for adhesion proteins and cytokines (b) Preparation of NRP+I and schematic illustration of chemo-immunotherapy. (c) Schematic illustration of CXCR4-targeted Dox delivery by bioreducible dextrin nanogel in metastatic breast cancer. Reprinted with permission from (a) *ACS Biomater. Sci. Eng.* **2016**, *2*, 375–384, (b) *Nano Lett.* **2017**, *17*, 6366–6375, (c) *Biomacromolecules* **2017**, *18*, 1793–1802. Copyright 2016, 2017 American Chemical Society.

References

1. Kim, Y. H.; Webster, O. W. *J. Am. Chem. Soc.* **1990**, *112*, 4592–4593.
2. Sunder, A.; Hanselmann, R.; Frey, H.; Mu, R. *Macromolecules* **1999**, *32*, 4240–4246.
3. Sunder, A.; Frey, H.; Mülhaupt, R. *Macromol. Symp.* **2000**, *153*, 187–196.
4. Sunder, A.; Mülhaupt, R.; Haag, R.; Frey, H. *Adv. Mater.* **2000**, *12*, 235–239.
5. Wilms, D.; Stiriba, S.; Frey, H. *Acc. Chem. Res.* **2010**, *43*, 129–141.
6. Kainthan, R. K.; Muliawan, E. B.; Hatzikiriakos, S. G.; Brooks, D. E. *Macromolecules* **2006**, *39*, 7708–7717.
7. Frey, H.; Haag, R. *Mol. Biotechnol.* **2002**, *90*, 257–267.
8. Kainthan, R. K.; Janzen, J.; Levin, E.; Devine, D. V; Brooks, D. E. *Biomacromolecules* **2006**, *7*, 703–709.
9. Wurm, F.; Dingels, C.; Frey, H.; Klok, H. *Biomacromolecules* **2012**, *13*, 1161–1171.
10. Schull, C.; Nuhn, L.; Mangold, C.; Christ, E.; Zentel, R.; Frey, H. *Macromolecules* **2012**, *45*, 5901–5910.
11. Mohammadifar, E.; Bodaghi, A.; Dadkhahtehrani, A.; Kharat, A. N.; Adeli, M.; Haag, R. *ACS Macro Lett.* **2017**, *6*, 35–40.
12. Weinhart, M.; Gr, D.; Enders, S.; Dernedde, J.; Haag, R. *Biomacromolecules* **2011**, *12*, 2502–2511.
13. Das, P.; Jana, N. R. *ACS Appl. Mater. Interfaces* **2014**, *6*, 4301–4309.
14. Liu, J.; Pang, Y.; Huang, W.; Zhu, Z.; Zhu, X.; Zhou, Y.; Yan, D. *Biomacromolecules* **2011**, *12*, 2407–2415.
15. Zhang, P.; Zhang, H.; He, W.; Zhao, D.; Song, A.; Luan, Y. *Biomacromolecules* **2016**, *17*, 1621–1632.
16. Zhou, M.; Qian, Z.; Chen, L.; Kaplan, D. L.; Xia, X. *Biomacromolecules* **2016**, *17*, 3508–3515.

17. Feng, C.; Lu, G.; Li, Y.; Huang, X. *Langmuir* **2013**, *29*, 10922–10931.

18. Kainthan, R. K.; Janzen, J.; Levin, E.; Devine, D. V; Brooks, D. E. *Biomacromolecules* **2006**, *7*, 703–709.

19. Wilms, D.; Stiriba, S.; Frey, H. *Acc. Chem. Res.* **2010**, *43*, 129–141.

20. Wurm, F.; Klos, J.; Ra, H. J.; Frey, H. *J. Am. Chem. Soc.* **2009**, *131*, 7954–7955.

21. Lee, S.; Saito, K.; Lee, H.; Lee, M. J.; Shibasaki, Y.; Oishi, Y.; Kim, B. *Biomacromolecules* **2012**, *13*, 1190–1196.

22. Donskyi, I. S.; Achazi, K.; Wycisk, V.; Licha, K.; Adeli, M.; Haag, R. *Langmuir* **2017**, *33*, 6595–6600.

23. Sisson, A. L.; Steinhilber, D.; Rossow, T.; Welker, P.; Licha, K.; Haag, R. *Angew. Chem. Int. Ed.* **2009**, *48*, 7540–7545.

24. Zhang, X.; Malhotra, S.; Molina, M.; Haag, R. *Chem. Soc. Rev.* **2015**, *44*, 1948–1973.

25. Donskyi, I. S.; Achazi, K.; Wycisk, V.; Licha, K.; Adeli, M.; Haag, R. *Langmuir* **2017**, *33*, 6595–6600.

26. Sisson, A. L.; Haag, R. *Soft Matter* **2010**, *6*, 4968–4975.

27. Sasaki, Y.; Akiyoshi, K. *Chem. Rec.* **2010**, *10*, 366–376.

28. Yu, Z.; Sun, J.; Pan, C.; Hong, C. *Chem. Commun.* **2012**, *48*, 5623–5625..

29. Nishimura, T.; Takara, M.; Mukai, S.; Sawada, S.; Sasaki, Y.; Akiyoshi, K. *Chem. Commun.* **2015**, *52*, 1222–1225.

30. Liu, B.; Thayumanavan, S. *J. Am. Chem. Soc.* **2017**, *139*, 2306–2317.

31. Chen, W.; Zheng, M.; Meng, F.; Cheng, R.; Deng, C.; Feijen, J.; Zhong, Z. *Biomacromolecules* **2013**, *14*, 1214–1222.

32. Ryu, J. H.; Jiwpanich, S.; Chacko, R.; Bickerton, S.; Thayumanavan, S. *J. Am. Chem. Soc.* **2010**, *132*, 8246–8247.

33. Unpublished.

34. Cao, Z.; Zhou, X.; Wang, G. *ACS Appl. Mater. Interfaces* **2016**, *8*, 28888–28896.

35. Vermonden, T.; Censi, R.; Hennink, W. E. *Chem. Rev.* **2012**, *112*, 2853–2888.

36. Smith, M. H.; Lyon, L. A. *Acc. Chem. Res.* **2012**, *45*, 985–993.

37. Li, Y.; Maciel, D.; Rodrigues, J.; Shi, X.; Tomas, H. *Chem. Rev.* **2015**, *115*, 8564–8608.

38. Hashimoto, Y.; Mukai, S.; Sawada, S.; Sasaki, Y.; Akiyoshi, K. *ACS Biomater. Sci. Eng.* **2016**, *2*, 375–384.

39. Song, Q.; Yin, Y.; Shang, L.; Wu, T.; Zhang, D.; Kong, M.; Zhao, Y.; He, Y.; Tan, S.; Guo, Y.; Zhang, Z. *Nano Lett.* **2017**, *17*, 6366–6375.

40. Zhang, F.; Gong, S.; Wu, J.; Li, H.; Oupicky, D.; Sun, M. *Biomacromolecules* **2017**, *18*, 1793–1802.

Part 2. Architecture-Controlled Synthesis of Redox-Degradable Hyperbranched Polyglycerol Block Copolymers and the Structural Implications of their Degradation

1. Introduction

Hyperbranched polyglycerol (PG) is one of the most popular hyperbranched polymers, which possess randomly branched structure with a large number of hydroxyl groups.[1,2] Owing to their excellent immunogenicity, biocompatibility and the large number of potential sites for more conjugation, PGs and their derivatives have appealed increasing interests for use in biomedical applications like polymer therapeutics, proteomics and human serum albumin substitutes.[3–8] Furthermore, hyperbranched PGs can be synthesized by a facile one-pot synthesis, even up to the kilogram scale, which guaranteed their successful development to industrial areas.[9,10] PGs are commonly prepared by the anionic ring-opening multi branching polymerization of glycidol, which can lead to a wide range of craved molecular weights from 1000 to 1,000,000 with low polydispersity. To build PGs with versatile functionality and diverse architectures, many functional epoxide monomers have been progressed, such as ethoxy ethyl glycidyl ether (EEGE), ethoxy vinyl glycidyl ether, allyl glycidyl ether (AGE).[11–18] These monomers can be copolymerized to produce PGs with various structures. For example, use of the protected glycidol monomer or EEGE monomer facilitate to diverse architectures like linear or linear hyperbranched PGs.[12,13] To introduce various functionalities, Mattson et al. have installed AGE for the subsequent functionalization via thiol-ene click chemistry.[18] Moreover, stimuli responsive epoxide monomers can be reported to yield degradable, hyperbranched PGs with fancy functionality. Particularly, to fulfill the demands of developed applications, materials based on PG that are biocompatible yet degradable under certain conditions are highly valuable. In ways that, redox- degradable disulfide groups and acid-cleavable ketal groups can be integrated into the monomer to yield a series of hyperbranched PGs that are degradable under certain stimuli.[19–21]

Determining degradable linkage groups or moieties within the polymer is an important matter; moreover, the investigation of the degradation products can give insight into explaining the specific structure of the polymers before degradation. As a result, studies on diversities of degradable polymers and their products have been commonly directed (Scheme 1).[22–25] Comparing to the many kind of research on the degradation of linear polymers, there have been rarely systematic report on the preparation and degradation of (hyper)branched polymers, owing to its structural complexity. Lately, some researchers studied the degradation of hyperbranched and brush polymers, for instance, Engler et al. have introduced polycarbonate based on brush polymers containing cleavable disulfide-linked side chains and their related products.[26] Furthermore, Rikkou-Kalourkoti et al. reported the synthesis and degradation of thermolyzable hyperbranched polymers containing thermolyzable acylal group.[27] Our group has lately reported the redox-responsive hyperbranched polyglycerols (PSSG) and degradation of products made from the copolymerization with glycidol monomer.[21] Nevertheless, the investigation of random copolymer system which the sequence of polymerization was not controlled was limited. Against the random copolymer, the location of disulfide linkage within the hyperbranched polymers has an important influence after the degradation. In conclusion, in continuation of our investigation into hyperbranched PGs for biomedical applications, we synthesized a series of redox-responsive hyperbranched PG-based polymers containing a disulfide containing monomer, 2-((2-(oxiran-2 ylmethoxy)ethyl)disulfanyl)ethan- 1-ol (SSG), to yield PSSG homopolymers and block copolymers with a non- degradable glycerol (G) monomer. Hyperbranched block copolymers of P(SSG-*b*-G) and P(G-*b*-SSG) with controlled molecular weights and relatively low polydispersity were synthesized by anionic ring-opening multibranching polymerization. We also revealed the specific structure of the degradation products from homopolymers and block copolymers of hyperbranched redox-responsive PGs under redox conditions using ^{1}H NMR and GPC measurements. As a result, we investigated the outstanding biocompatibility of PSSG, P(G-*b*- SSG) and P(SSG-*b*-G) through cell viability assays.

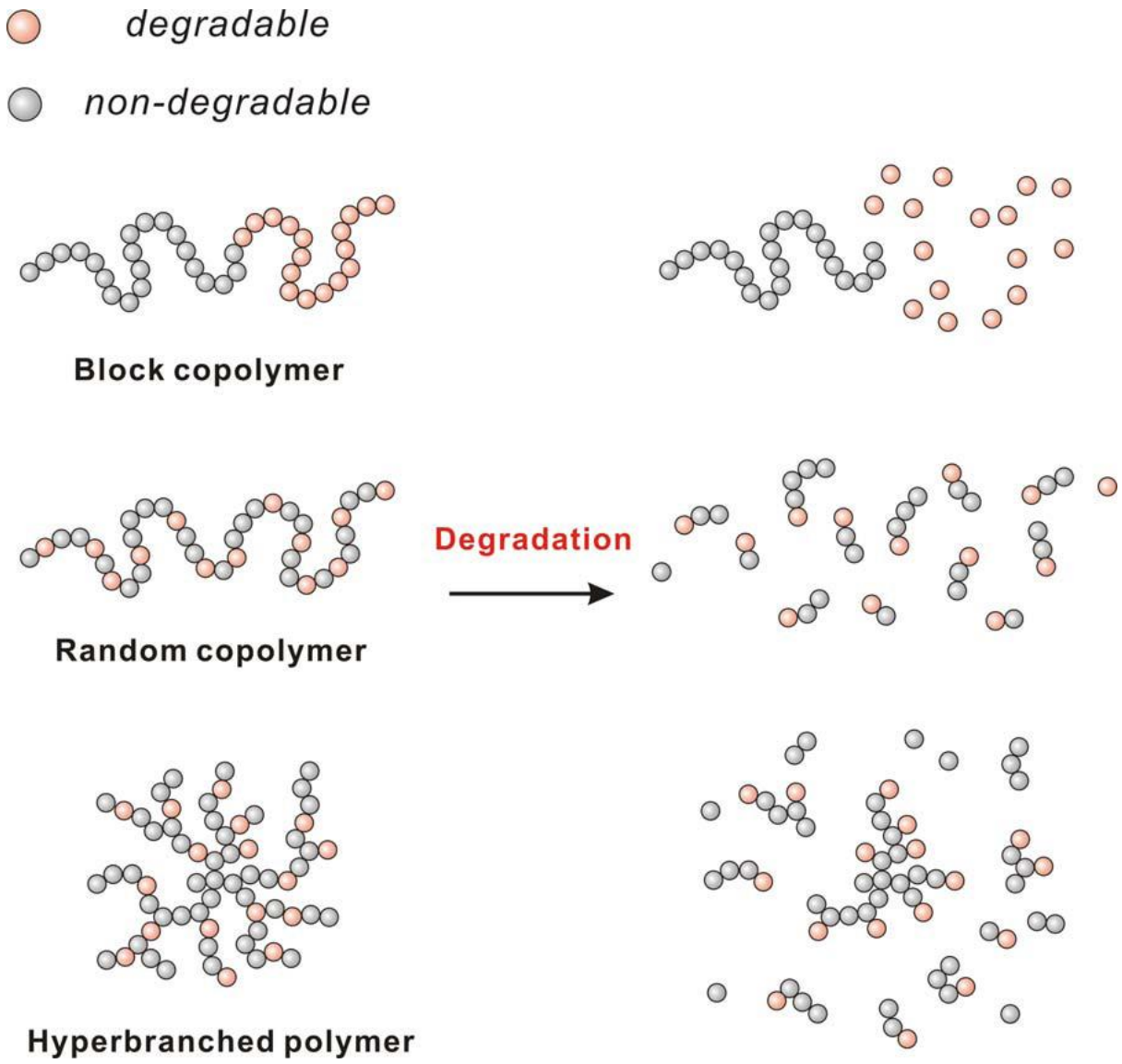

Scheme 1. Degradation structure depending on the type of polymers.

2. Experimental section

2.1. Materials

All reagents and solvents were purchased from either Sigma Aldrich or Acros and used as received unless otherwise stated. Chloroform-d1 and deuterium oxide were purchased from Cambridge Isotope Laboratory.

2.2. Characterization

^{1}H NMR spectra were acquired using a VNMRS 600 spectrometer operating at 600 MHz using $CDCl_3$ and D_2O as solvents. The number- and weight-averaged molecular weight and molecular weight distribution were measured by gel permeation chromatography (GPC, Agilent Technologies 1200 series) using polystyrene as a standard in DMF. Measurements were carried out at 30 °C with a flow rate of 1.00 mL/min. Differential scanning calorimetry (DSC) was performed using a DSC Q200 model from TA Instruments in the temperature range of 280 to 100 °C at a heating rate of 10 K/min under nitrogen. A UV-Vis spectrophotometer (UV- 2550, Shimadzu) was used to measure the absorbance of iodine for the volumetric titration of free thiols.

2.3.Synthesis of SSG (Monomer), PSSG (Homopolymer), and P(G-*co*-SSG) (Copolymer)

SSG monomer, PSSG homopolymer, and P(G-*co*-SSG) copolymers were prepared according to the previously reported method.[21]

2.4. Synthesis of Poly(glycerol-block22-{2-[2-(oxiran-2-ylmethoxy)ethyl] disulfanyl} ethanol) (P(G_{130}-*b*-SSG_{80}) Block Copolymer, Polymer 6)

Trimethylolpropane (TMP) (24 mg, 0.179 mmol) was placed in a two-neck round-bottom flask. Potassium methoxide in methanol (25 wt%, 20 µL, 0.0678 mmol) was diluted with 0.70 mL of methanol and then added to the flask and stirred for 30 min at room temperature under an argon atmosphere. Excess methanol was removed using a rotary evaporator and the remaining product was dried in a vacuum oven (90 °C, 3 h) to yield the initiator as a white salt. The flask was then purged with argon and heated to 90 °C. Then, glycidol (G) monomer (1.72 g, 23.2 mmol) was added dropwise over 6 h using a syringe pump. After complete addition of the monomer, the reaction was allowed to continue for an additional 1 h to yield the PG macroinitiator. Then, to this solution, SSG monomer (3.01 g, 14.3 mmol) was added dropwise

over 6 h using a syringe pump. After complete addition of the monomer, the reaction was allowed to continue for an additional 1 h. The resulting P(G-*b*-SSG) polymer was dissolved in 1.0 mL of methanol and the homogeneous polymer solution was precipitated into excess diethyl ether and washed twice with diethyl ether. Finally, the resulting polymer was dried under vacuum at 60 °C for 2 days. The M_n of polymer 6 was 18,400 g/mol, as calculated from the NMR data shown in **Figure 2(a)** using the following equation: Number of repeating units (SSG) = 56.31 (integration value) * 3 (number of protons of TMP (methyl, 3H))/4 (number of protons neighboring the disulfide moiety of SSG (4H)) = 42, number of repeating units (G)5[339.92 (integration value) * 3 (number number of protons of TMP (methyl, 3H)) – {(42 (number of SSG repeating units) * 9 (number of protons of SSG except those that are adjacent to the disulfide moiety (9H))) – 6 (number of protons of TMP (ether, 6H))}]/5 (number of protons of the G monomer (5H)) = 127; M_n = 74.08 (molecular weight of the G monomer) * 127 + 210.31 (molecular weight of the SSG monomer) * 42 + 134.17 (molecular weight of TMP) = 18,400.

2.5. Synthesis of Poly(glycerol-block22-{2-[2-(oxiran-2- ylmethoxy)ethyl] disulfanyl} ethanol) (P(SSG_{30}-*b*-G_{100}) Block Copolymer, Polymer 9)

P(SSG_{30}-*b*-G_{100}) block copolymer was synthesized using the same strategy to prepare the P(G-*b*-SSG) block copolymers; however, the monomer addition sequence was reversed. The reaction mixture comprised trimethylolpropane (TMP) (24 mg, 0.179 mmol), potassium methoxide in methanol (25 wt%, 20 µL, 0.0678 mmol) in 0.70 mL of methanol, SSG monomer (1.13 g, 5.36 mmol), and glycidol (G) monomer (1.32 g, 17.9 mmol). The M_n of polymer 9 was 14,700 g/ mol, as calculated from the NMR data shown in **Figure 2(b)** using the following equation: Number of repeating units (SSG) = 30.53 (integration value) * 3 (number of protons of TMP (methyl, 3H))/4 (number of protons neighboring the disulfide moiety of SSG (4H)) = 23, number of repeating units (G) = [314.24 (integration value) * 3 (number of protons of TMP (methyl, 3H)) – {(31 (number of SSG repeating units considering only PSSG core) * 9 (number of protons of SSG except those that are adjacent to the disulfide moiety (9H))) – 6 (number of protons of TMP (ether, 6H))}]/5 (number of protons of the G monomer (5H)) = 131; M_n = 74.08 (molecular weight of the G monomer) * 131 + 210.31 (molecular weight of the SSG monomer) * 23 + 134.17 (molecular weight of TMP) = 14,700.

2.6. Characterization of Free Thiol by Iodine Titration

For titration experiments, an aqueous solution of mercaptoethanol (10.0 mM) was used to draw a standard titration curve. Specifically, 5.0 μL of aqueous iodine solution (0.10 mM) was added dropwise to a solution of mercaptoethanol with stirring while monitoring the UV-Vis absorbance at 287 nm and 351 nm. This titration measurement afforded a standard calibration curve for the iodine titration of free thiol in solution.

2.7. Polymer Degradation

Degradation of PSSG by disulfide reduction was studied by GPC. Dithiothreitol (DTT, 2 equiv of disulfide) was added to solutions of the PSSG homopolymer, P(G-*b*-SSG), and P(SSG-*b*- G) block copolymers in DMF and the samples were analyzed using GPC in DMF. The molecular weight and PDI were measured and the results of before and after DTT treatment were compared.

2.8. Cytotoxicity Assay

MTT assay was performed according to the previously reported method.[21]

3. Results and discussion

3.1. Synthesis of Hyperbranched Block Copolymers

We prepared two different types of hyperbranched block copolymers, P(G-*b*-SSG) and P(SSG-*b*-G), by adding the two monomers in a sequential difference (Figure 1). In this report, we synthesized hyperbranched block copolymers using synthetic redox-degradable monomers such as nondegradable glycidol (G) and SSG. Hyperbranched AB block copolymer can make striking different structures by changing the order of monomer addition during synthesis. To regulate the degradation kinetics, we changed the order of polymerization of the two respective monomers; for example, in the case of P(G-*b*-SSG), after the hyperbranched PG macroinitiator was synthesized, SSG was added to make the P(G-*b*-SSG) copolymer. All polymers were prepared by anionic ring-opening multibranching polymerization, prepared by the reaction of TMP as initiator and potassium methoxide as a base.[9] As reported in previous studies, the slow monomer addition method (SAM) can be able to use in the synthesis of hyperbranched polymers in a controlled manner.[8,21] Successful syntheses of homopolymers and two types of block copolymers were confirmed using ^{1}H NMR, GPC, and DSC measurement (Table 1). All synthesized PSSG-based polymers were water-soluble polar organic solvents-soluble like DMF, methanol, and DMSO. The successful polymerization was identified with disappearance of epoxide signal by G and SSG in the ^{1}H NMR spectra and the characteristic peaks corresponding to the methylene groups adjacent to the disulfide moiety (peaks labeled c at 2.9 - 3.1 ppm) and polyether backbone signals (peaks marked d at 3.4 - 4.2 ppm) (Figure 2). In Figure 2a, we found substantial variation in the disulfide signal upon additional polymerization of the SSG monomer to produce the hyperbranched block copolymer, P(G-*b*-SSG). Even though new peaks were not watched for P(SSG-*b*-G), the ^{1}H NMR intensity of signals coming about the polyether backbone became stronger after addition of monomer G, presenting the of growth the polyether backbone during polymerization of G (Figure 2b). Commonly, we confirmed relatively high concurrence between the target and calculated molecular weights of homopolymers of PG and PSSG; though, there are some differences between polymer composition with feed ratio and NMR for the two types of hyperbranched block copolymers (Table 1). Our previous study in situ ^{13}C NMR have revealed that the SSG monomer has relatively low conversion (40– 55%) compared to pure G monomer due to its low reactivity. This discrepancy in reactivity could be affected to the structure of the disulfide spacer within SSG, which can impede the nucleophilic attack at epoxide, then decrease the reactivity of SSG

during polymerization. In contrast, we explained the lower intensity of disulfide signal after addition of G having new peaks at 2.8 to 2.9 ppm, which could be affected to the methylene group close to the sulfenyl ester groups and thiol from side-reactions of the disulfide group. For example, we observed that the $PSSG_{30}$ (polymer 2) became $P(SSG_{23}$-*b*-$G_{131})$ (polymer 9) after polymerization with G monomer. This result certainly implies the happening of a side reaction including the depolymerization of disulfide bonds during the post-polymerization with more reactive G monomer. It is decided that the making alkoxide group (RO_2) of the G monomer reacts with the disulfide group (R'SSR'') to produce thiolate (R'S-) and sulfenyl esters (ROSR'') during the postpolymerization with G, which will finally disintegrate into thiols (R'SH and R''SH) and alcohol (ROH).[28,29] To investigate the side reactions of PSSG during the polymerization, we checked free thiol titration experiments by oxidizing thiol with iodine.[30,31] It is well-known that hydrophilic thiols can be oxidized to disulfide by aqueous iodine and results in the appearance characteristic UV-vis absorbance peaks at 287 and 351 nm.

$$2RSH + I_2 \rightarrow RSSR + 2HI,\ I_2 + HI \rightarrow H^+ + I_3^-$$

on the basis of the reactions existed above, we confirmed the amounts of free thiols in PSSG homopolymers and block copolymers of P(G-*b*-SSG) and P(SSG-*b*-G) using mercaptoethanol as a reference standard (Table 2). We confirmed that both the PSSG homopolymer and P(G-*b*-SSG) block copolymer had a little thiol content of around 10% free thiol to disulfide groups (i.e., SH/SS ratio) owing to the side reaction during the polymerization. On the other hand, the P(SSG-*b*-G) block copolymer had a relatively high SH/SS ratio with a broad range (14 - 129%). Moreover, we checked that the SH/SS ratio of P(SSG-*b*-G) depended on the G/SSG ratio; In other words, a high G/SSG ratio results a higher SH/ SS ratio. Furthermore, two facts regarding this results happened: (i) even though $P(SSG_{30}$-*b*-$G_{50})$ (polymer 8) and $P(SSG_{30}$-*b*-$G_{100})$ (polymer 9) were polymerized from the same $PSSG_{30}$ macroinitiator (polymer 2), $P(SSG_{30}$-*b*-$G_{100})$ has a higher SH/SS ratio than $P(SSG_{30}$-*b*-$G_{50})$, and (ii) despite $P(SSG_{14}$-*b*-$G_{100})$ (polymer 7) and $P(SSG_{30}$-*b*-$G_{100})$ (polymer 9) with the same G composition, $P(SSG_{14}$-*b*-$G_{100})$ has a higher SH/SS ratio owing to its high G/SSG ratio. The GPC results explain that the polymerization of hyperbranched block copolymers from their each macroinitiators, PG_{130} and $PSSG_{30}$, was successfully synthesized, and the hyperbranched polymers had relatively low molecular weight distribution values (M_w/M_n<1.54) (Table 1). On the other hand, there is distinction between the molecular weights calculated from NMR and those obtained from GPC. This result can be explained because globular hyperbranched structure of hyperbranched PG

did not contribute to the overall hydrodynamic radius of the polymers. Moreover, we used DSC measurements to confirm the structures of hyperbranched block copolymers and their thermal properties (Figure 3). PGs are non-crystalline, flexible polymers that have glass transition temperatures (T_g) in the range from 219 to 226 °C. However, the PSSG homopolymer has a pretty lower T_g than those of the PGs; for instance, it has a range of between 248 to 255 °C.[18] The lower T_g of PSSG can be explained for by two reasons: (i) the longer-CH_2CH_2-S-S-CH_2CH_2- spacer unit in the PSSG monomer generates a loose structure of polymer compared to the dense structure of that of PG and (ii) lower polarity and weak hydrogen bonding in PSSG can effect in free motion of the polymer chain. The T_g's of the hyperbranched block copolymers of P(G-*b*-SSG) exist between those of PG and PSSG. For instance, after polymerization to form hyperbranched P(G_{130}-*b*-SSG_{80}), the T_g of PG_{130} (225 °C) shifted to 233 °C. Furthermore, the T_g of $PSSG_{30}$ (238 °C) increased to 231 °C in the P(SSG_{30}-*b*-G_{100}) copolymer. It is note that we confirmed only single T_g from the PSSG from hyperbranched block copolymer compared to the two independent T_g's of linear block copolymers. We postulate that this result is attributed to miscibility of PG and PSSG, and, more importantly, its globular hyperbranched structure even in the segregated block copolymer architecture, constraint phase separation between two blocks. we confirmed that a simple blend of two homopolymers retained two separate T_g's of the respective homopolymers.

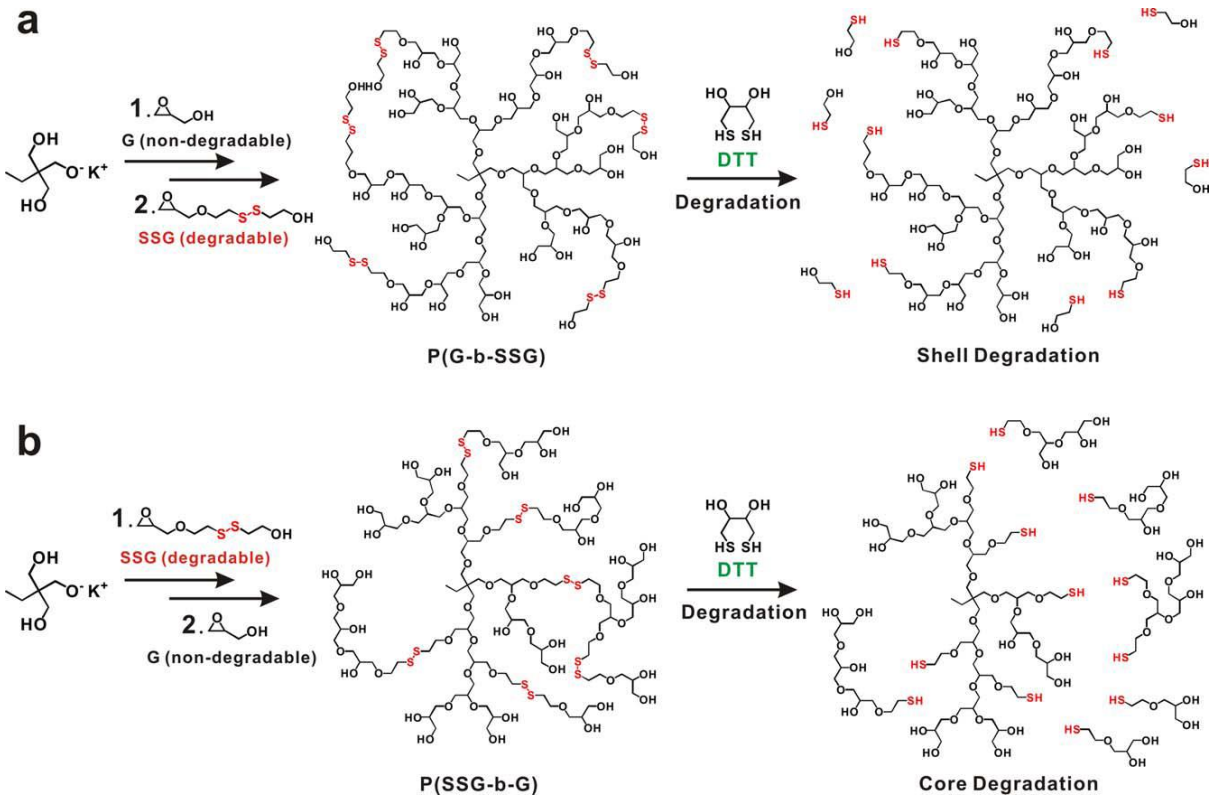

Figure 1. Synthetic pathway and degradation structure of two types of redox-degradable hyperbranched block copolymers; (a) shell degradable P(G-*b*-SSG) and (b) core degradable P(SSG-*b*-G).

Table 1. Characterization data for all homo- and copolymers synthesized in this study.

No.	Polymer Composition (Target)	Polymer Composition (NMR)[a]	M_n (Target)	%SSG (Target)	M_n (NMR)[a]	%SSG (NMR)[a]	M_n (GPC)[b]	M_n/M_w (GPC)[b]	T_g (DSC)
1	PG_{150}	PG_{147}	11,200	0	11,000	0	9,600	1.28	−25
2	$PSSG_{30}$	$PSSG_{31}$	6,440	100	6,650	100	4,230	1.39	−38
3	P(G_{167}-*co*-SSG_{56})	P(G_{114}-*co*-SSG_{48})	24,190	25.1	18,700	29.6	15,800	1.28	−34
	P(G-*b*-SSG)								
4	P(G_{50}-*b*-SSG_9)	P(G_{52}-*b*-SSG_5)	6,210	15.3	5,040	8.8	3,760	1.23	−35
5	P(G_{100}-*b*-SSG_{10})	P(G_{100}-*b*-SSG_4)	9,640	9.1	8,380	3.9	7,890	1.54	−30
6	P(G_{130}-*b*-SSG_{80})	P(G_{127}-*b*-SSG_{42})	26,590	38.1	18,400	24.9	12400	1.27	−33
	P(SSG-*b*-G)								
7	P(SSG_{14}-*b*-G_{100})	P(SSG_3-*b*-G_{97})	10,490	12.3	7,950	3.0	7,700	1.35	−32
8	P(SSG_{30}-*b*-G_{50})	P(SSG_{28}-*b*-G_{65})	10,150	37.5	10,800	30.1	5,680	1.39	−33
9	P(SSG_{30}-*b*-G_{100})	P(SSG_{23}-*b*-G_{131})	13,850	23.1	14,700	14.9	6,470	1.34	−31

[a] Determined via ^{1}H NMR spectroscopy. [b] Obtained from GPC-RI in DMF with a polystyrene standard.

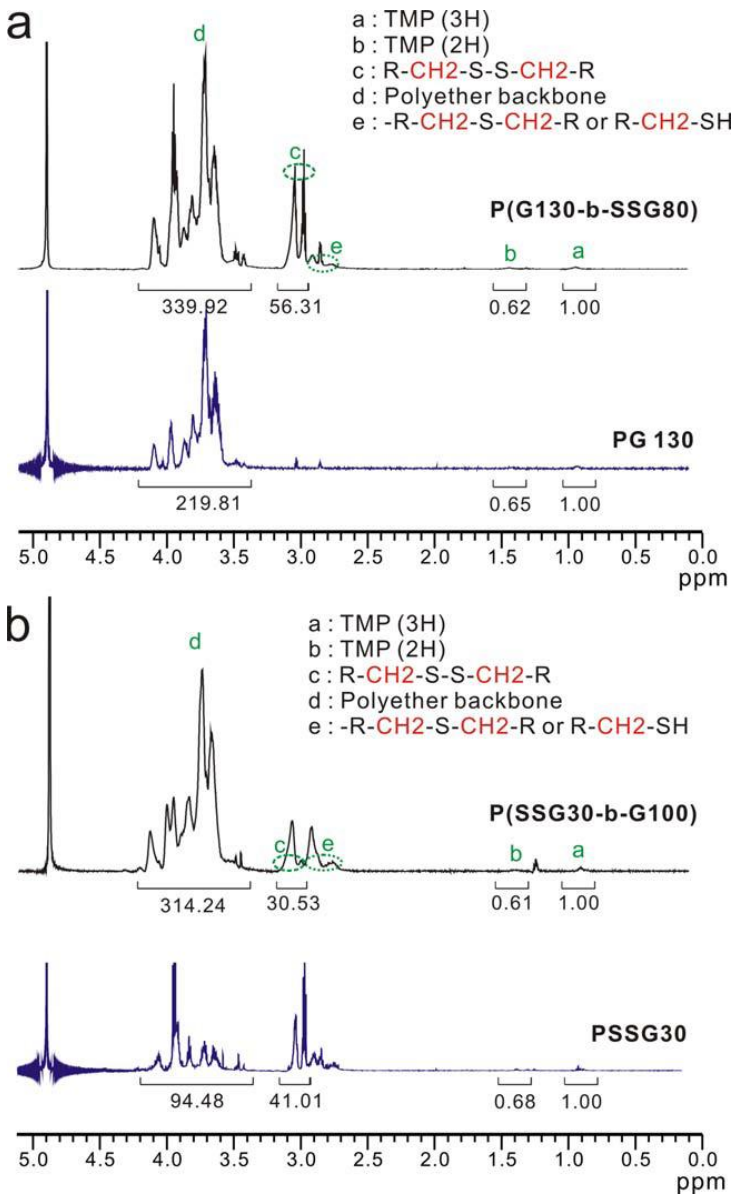

Figure 2. ^{1}H NMR spectra before and after addition of the second monomer to confirm the successful synthesis of the hyperbranched block copolymers of (a) P(G_{130}-*b*-SSG_{80}) and (b) P(SSG_{30}-*b*-G_{100}).

Table 2. Characterization data for the side reactions of PSSG-based copolymers.

No	Polymer Composition (Target)	Polymer Composition (NMR)[a]	G/SSG Ratio (Target)	G/SSG Ratio (NMR)[a]	No. SH in a Polymer Chain (UV-Vis)[b]	No. SS in a Polymer Chain (NMR)[b]	SH/SS%
	$PSSG_{10}$	$PSSG_{9}$			0.63	9	7.0
2	$PSSG_{30}$	$PSSG_{31}$			0.78	31	2.5
	$PSSG_{50}$	$PSSG_{53}$			1.30	53	2.4
	P(G-*b*-SSG)						
4	$P(G_{50}$-*b*-$SSG_{9})$	$P(G_{52}$-*b*-$SSG_{5})$	5.55	10.40	0.58	5	11.6
5	$P(G_{100}$-*b*-$SSG_{10})$	$P(G_{100}$-*b*-$SSG_{4})$	10.00	25.00	0.23	4	5.7
6	$P(G_{130}$-*b*-$SSG_{80})$	$P(G_{127}$-*b*-$SSG_{42})$	1.62	3.02	1.93	42	4.6
	P(SSG-*b*-G)						
7	$P(SSG_{14}$-*b*-$G_{100})$	$P(SSG_{3}$-*b*-$G_{97})$	7.14	32.33	3.88	3	129.3
8	$P(SSG_{30}$-*b*-$G_{50})$	$P(SSG_{28}$-*b*-$G_{65})$	1.66	2.32	3.94	28	14.1
9	$P(SSG_{30}$-*b*-$G_{100})$	$P(SSG_{23}$-*b*-$G_{131})$	3.33	5.69	10.12	23	44.0

[a] Determined via ^{1}H NMR spectroscopy. [b] Measured using UV-Vis spectroscopy by plotting the intensity at a wavelength of 351 nm.

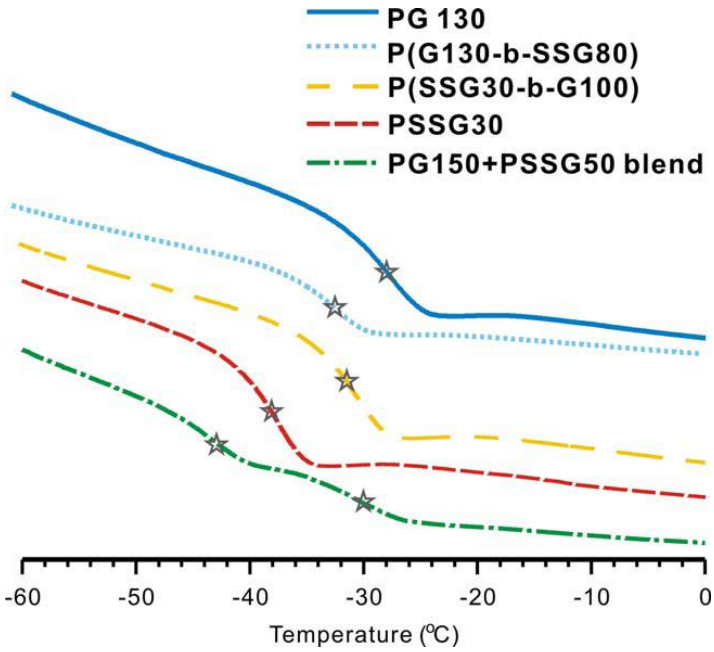

Figure 3. DSC curves for PG_{130} (blue), P(G_{130}-*b*-SSG_{80}) (sky blue), P(SSG_{30}-*b*-G_{100}) (yellow), $PSSG_{30}$ (red), and a simple blend of PG_{150} and $PSSG_{50}$ homopolymers (green). Star marks indicate the glass transition temperatures (T_g) for each polymer.

3.2.Degradation Study of Two Types of Hyperbranched Block Copolymers

The presence of disulfide bonds in the polymer allows their degradation under redox condition. SSG has an important advantage over other degradable epoxide monomers for studies of degradable PGs. Especially, SSG can be homopolymerized with almost 100% conversion, while other degradable monomers originally display only low conversions (ca. 20%) during polymerization. By utilizing this advantage, we easily synthesized P(G-*b*-SSG) and P(SSG-*b*-G) block copolymers by changing the sequence of addition of the monomers, allowing us to research the structures of the degradation PSSG with respect to the architecture of the block copolymer. First of all, we checked the degradation of the shell-degradable hyperbranched block copolymer of P(G-*b*-SSG). For this polymer, we anticipated that the outer shell would be degraded while decreasing in molecular weight. As shown in Figure 4a, we confirmed that the molecular weight of polymer 6 decreased slightly from 12,440 to 10,090 g/mol after degradation. Although GPC measurement with PS standards retains intrinsic limitation in determining the exact molecular weight of hyperbranched polyglycerol systems, interestingly, the difference in their molecular weights corresponds to that of the degradation products (i.e., 30 mercaptoethanol molecules). Therefore, we concluded that P(G-*b*-SSG) releases mercaptoethanol from the outer shell on degradation. In order to observe the complex degradation of the core degradable hyperbranched block copolymer P(SSG-*b*-G), we first studied the degradation mechanism of the PSSG homopolymer. In our previous work, we gained mechanistic insights on the degradation of PSSG polymers.[21] These were based on the presence of two possible reaction sites in SSG: the secondary alcohol and the disulfide linked primary alcohol.[18] Here, we have further studied the detailed structure of the PSSG homopolymers by NMR spectroscopy to study polymer degradation. During polymerization of the SSG monomer, there are two possible reaction routes for the hydroxyl groups that affect the direction of propagation of the growing polymer chain. For example, if a secondary alkoxide group is propagated, the polymer chain attaches to an epoxide unit and a linear 1,3-unit ($L_{1,3}$) is generated; in contrast, a linear 1,11-unit ($L_{1,11}$) is formed if a primary alkoxide reacts (Figure 5). Although it is reported that the primary alkoxides ($L_{1,4}$) are almost threefold more reactive than secondary alkoxides ($L_{1,3}$) for anionic ring-opening multibranching polymerizations of a pure PG system,[9] PSSG shows the opposite tendency, to our surprise. Specifically, in the case of $PSSG_{30}$, we found that the secondary alcohol ($L_{1,3}$) is 1.71 times more reactive than the primary alcohol ($L_{1,11}$). We propose that this observed difference in

reactivity is mainly due to the relatively slow proton exchange that occurs in the long spacer unit of $RCH_2CH_2S\text{-}SCH_2CH_2OH$; thus, to exchange the proton, attack by an oxyanion is preferred entailing at the neighboring epoxide monomer. After degradation, a large core segment is left with a molecular weight of 2281 g/mol, which closely corresponds to the value derived from GPC (2780 g/mol), as shown in Figure 4b.

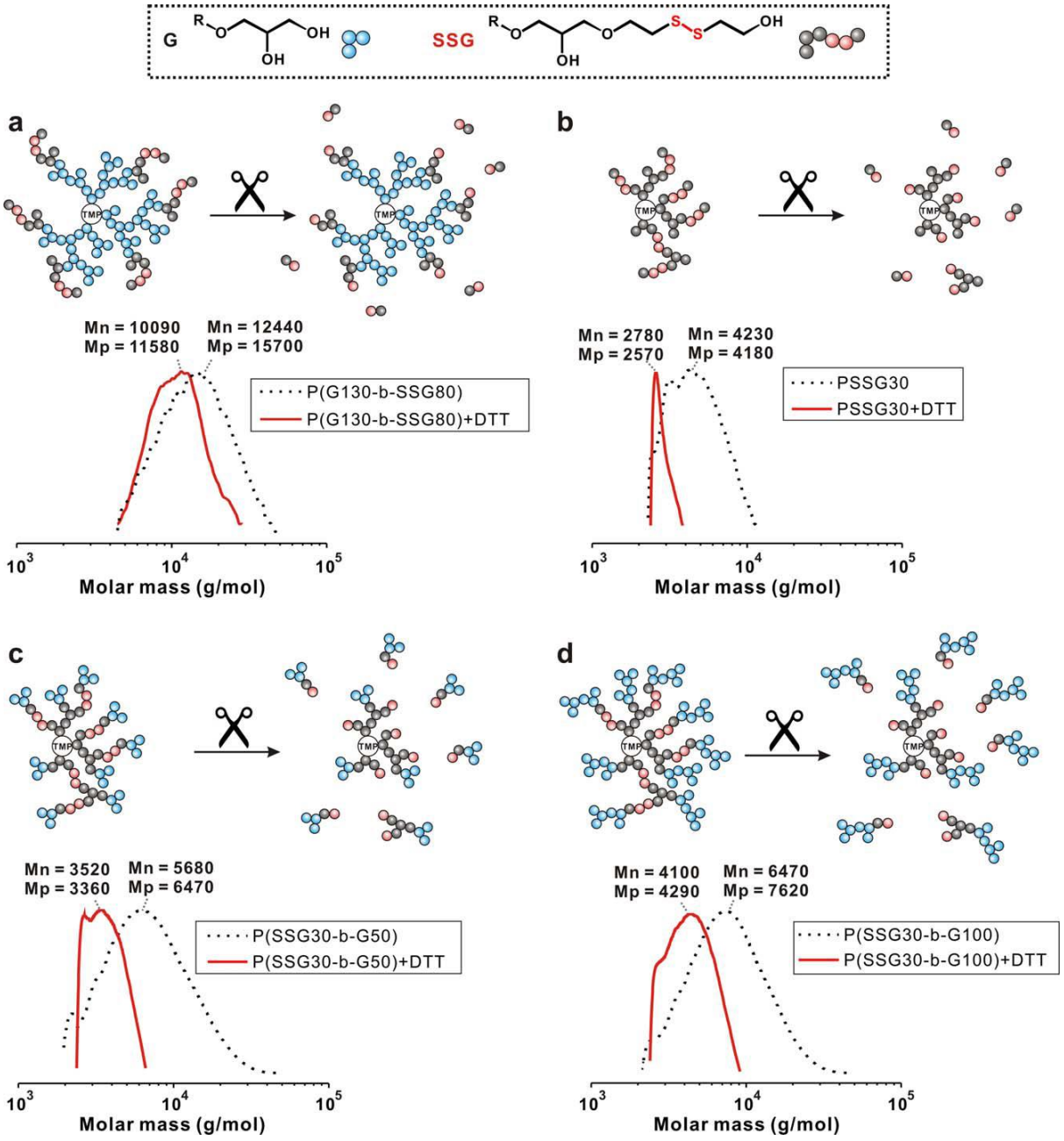

Figure 4. Schematic degradation structure of PSSG polymers and the corresponding GPC traces of (a) P(G_{130}-*b*-SSG_{80}), (b) $PSSG_{30}$, (c) P(SSG_{30}-*b*-G_{50}), and (d) P(SSG_{30}-*b*-G_{100}) before (black curve) and after (red curve) degradation.

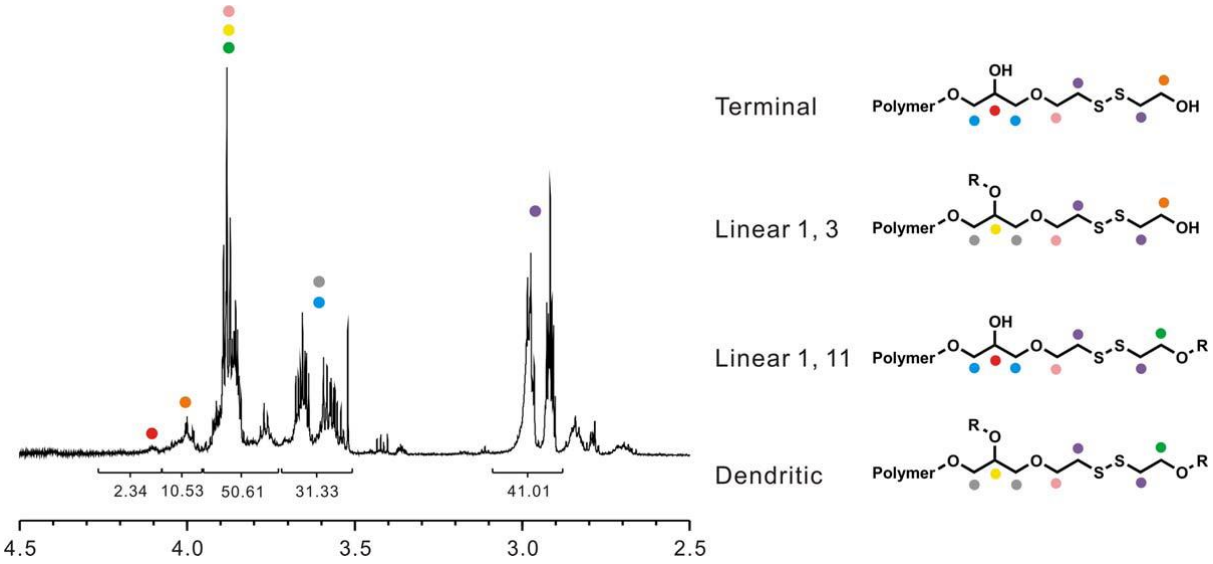

Figure 5. ^{1}H NMR spectra of $PSSG_{30}$ homopolymer and detailed assignments of the respective protons giving rise to these signals.

3.3.Biocompatibility Test

We confirmed the biocompatibility of $PSSG_{30}$, P(SSG_{30}-*b*-G_{50}), P(SSG_{30}-*b*-G_{100}), and P(G_{130}-*b*-SSG_{80}) to investigate their potential usages for biomedical application. We focused on differences in cell viability with respect to the location of the disulfide bonds in the hyperbranched polyglycerols even though our previous studies have reported that the SSG monomer does not have a side effect on cells when copolymerized with G. Cells treated to $PSSG_{30}$, P(SSG_{30}-*b*-G_{50}), and P(SSG_{30}-*b*-G_{100}), which located SSG within the core, showed high cell viability with increasing G content in Figure 6. This can be proved by the non-toxic PG chains that encircle the PSSG core as G content increases. The other way, P(G_{130}-*b*-SSG_{80}) causes cells to have more toxicity than P(SSG_{30}-*b*-G_{100}) because SSG is exposed at the outer shell. Moreover, disulfide bonds in P(G-*b*-SSG) stably remain nevertheless the unstable disulfide bond in P(SSG-*b*-G) can be converted to thiol or thioether under polymerization conditions, resulting to the higher biocompatibility of P(SSG-*b*-G) than P(G-*b*-SSG).

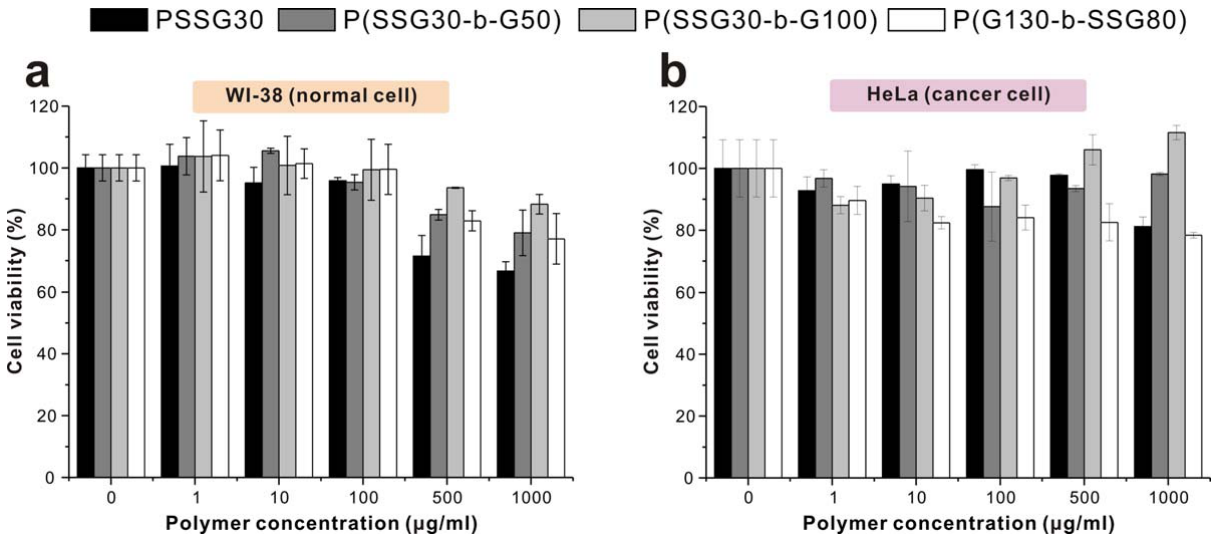

Figure 6. *In vitro* cell viability assays of $PSSG_{30}$ (black), $P(SSG_{30}$-*b*-$G_{50})$ (dark grey), $P(SSG_{30}$-*b*-$G_{100})$ (grey), and $P(G_{130}$-*b*-$SSG_{80})$ (white) polymers determined by MTT assay using (a) WI-38 (normal cell) and (b) HeLa (cancer cell).

4. Conclusion

PSSG homopolymers and block copolymers were successfully synthesized by anionic ring-opening polymerization using the redox-responsive monomer containing disulfide bonds and the non-degradable G monomer. The synthesized polymers were analyzed by ^{1}H NMR spectroscopy, GPC, and DSC measurements, and these confirmed well-controlled molecular weight and low polydispersity. Disulfide bond side reactions during polymerization, which are important in redox-responsive systems, were confirmed by free thiol titration experiments, which demonstrated that thiol groups produced by side reactions during polymerization exist within the final polymer. Moreover, we found that P(SSG-*b*-G) has more thiol groups than either PSSG or P(G-*b*-SSG). We also studied the structures of the degradation products of a series of redox degradable hyperbranched PGs using ^{1}H NMR, and GPC measurements. We found that the structure of the degradation products of P(G-*b*-SSG) and P(SSG-*b*-G) are different, and showed degradation mechanism. *In vitro* cytotoxicity studies verified the proper biocompatibility of hyperbranched redox degradable homo-, block copolymer. Finally, we expect that our research will progress the structural diversity of PG based polymers and help the understanding of the structure of degradable PG systems.

References

1. D. Wilms, S. E. Stiriba, H. Frey, *Acc. Chem. Res.* **2009,** *43*, 129–141.
2. H. Frey, R. Haag, R. *Rev, Mol. Biotechnol.* **2002,** *90*, 257–267.
3. A. Thomas, S. S. Müller, H. Frey, *Biomacromolecules* **2014,** *5*, 1935–1954.
4. R. K. Kainthan, J. Janzen, E. Levin, D. V. Devine, D. E. Brooks, *Biomacromolecules* **2006,** *7*, 703–709.
5. M. C. Lukowiak, S. Wettmarshausen, G. Hidde, P. Landsberger, V. Boenke, K. Rodenacker, U. Braun, J. F. Friedrich, A. A. Gorbushina, R. Haag, *Polym. Chem.* **2015,** *6*, 1350–1359.
6. R. K. Kainthan, J. Janzen, J. N. Kizhakkedathu, D. V. Devine, D. E. Brooks, *Biomaterials* **2008,** *29*, 1693–1704.
7. S. Lee, K. Saito, H. R. Lee, M. J. Lee, Y. Shibasaki, Y. Oishi, B. S. Kim, *Biomacromolecules* **2012,** *13*, 1190–1196.
8. S. Son, E. Shin, B. S. Kim, *Biomacromolecules* **2014,** *15*, 628– 634.
9. A. Sunder, R. Hanselmann, H. Frey, R. Mülhaupt, *Macromolecules* **1999,** *32*, 4240–4246.
10. R. A. Shenoi, D. E. Brooks, J. N. Kizhakkedathu, *J. Polym. ci. Part A: Polym. Chem.* **2013,** *51*, 2614–2621.
11. C. Mangold, F. Wurm, H. Frey, *Polym. Chem.* **2012,** *3*, 1714– 1721.
12. M. Erberich, H. Keul, M. Möller, *Macromolecules* **2007,** *40*, 3070–3079.
13. Y. Oikawa, S. Lee, D. H. Kim, D. H. Kang, B. S. Kim, K. Saito, S. Sasaki, Y. Oishi, Y. Shibasaki, *Biomacromolecules* **2013,** *14*, 2171–2178.
14. F. Paulus, D. Steinhilber, P. Welker, D. Mangoldt, K. Licha, H. Depner, S. Sigrist, R. Haag, *Polym. Chem.* **2014,** *5*, 5020– 5028.
15. C. Schüll, T. Gieshoff, H. Frey, *Polym. Chem.* **2013,** *4*, 4730– 4736.
16. B. F. Lee, M. J. Kade, J. A. Chute, N. Gupta, L. M. Campos, G. H. Fredrickson, E. J. Kramer, N. A. Lynd, C. J. Hawker, *J. Polym. Sci. Part A: Polym. Chem.* **2011,** *49*, 4498–4504.
17. A. Lee, P. Lundberg, D. Klinger, B. F. Lee, C. J. Hawker, N. A. Lynd, *Polym. Chem.* **2013,** *4*, 5735–5742.
18. K. M. Mattson, A. A. Latimer, A. J. McGrath, N. A. Lynd, P. Lundberg, Z. M. Hudson,

C. J. Hawker, *J. Polym. Sci. Part A: Polym. Chem.* **2015,** *53*, 2685–2692.

19. R. A. Shenoi, J. K. Narayanannair, J. L. Hamilton, B. F. Lai, S. Horte, R. K. Kainthan, J. P. Varghese, K. G. Rajeev, M. Manoharan, J. N. Kizhakkedathu, *J. Am. Chem. Soc.* **2012,** *134*, 14945–14957.
20. R. A. Shenoi, B. F. Lai, M. Imran ul-haq, D. E. Brooks, J. N. Kizhakkedathu, *Biomaterials* **2013,** *34*, 6068–6081.
21. S. Son, E. Shin, B. S. Kim, *Macromolecules* **2015,** *48*, 600– 609.
22. J. T. Wiltshire, G. G. Qiao, *Macromolecules* **2008,** *41*, 623– 631.
23. C. C. Chang, T. Emrick, *Macromolecules* **2014,** *47*, 1344– 1350.
24. J. T. Wiltshire, G. G. Qiao, *Macromolecules* **2006,** *39*, 9018– 9027.
25. R. Nicolaÿ, L. Marx, P. Hėmery, K. Matyjaszewski, *Macromolecules* **2007,** *40*, 9217–9223.
26. A. C. Engler, J. M. Chan, K. Fukushima, D. J. Coady, Y. Y. ang, J. L. Hedrick, *ACS Macro Lett.* **2013,** *2*, 332–336.
27. M. Rikkou-Kalourkoti, K. Matyjaszewski, C. S. Patrickios, *Macromolecules* **2012,** *45*, 1313–1320.
28. A. J. Parker, N. Kharasch, *Chem. Rev.* **1959,** *59*, 583–627.
29. R. G. Hiskey, A. J. Dennis, *J. Org. Chem.* **1968,** *33*, 2734– 2738.
30. J. P. Danehy, M. Y. Oester, *J. Org. Chem.* **1967,** *32*, 1491– 1495.
31. M. Desroches, S. Caillol, V. Lapinte, R. Auvergne, B. Boutevin, *Macromolecules* **2011,** *44*, 2489–2500.

Part 3. Reduction Triggered Self-Cross-Linked Hyperbranched Polyglycerol Nanogels

1. Introduction

Nanogels are aqueous dispersions of hydrogel particles in the nanometer range, which are formed from physically or chemically cross-linked polymeric networks.[1–3] Owing to the unique advantages that combine the characteristics of hydrogels and nanoparticles, nanogels are actively investigated as promising platforms for advanced biomedical applications.[4–8] In contrast to other self-assembled nanostructures, nanogels are more stable and have longer circulation times. Specifically, the development of nanogels in drug delivery could address a range of challenges to allow precise control over properties such as structure, size, surface functionality, hydrophilic/hydrophobic balance, and drug loading capacity.[9–12] When responsive polymers are exploited as building blocks for nanogels, smart nanogels can be prepared that stably encapsulate therapeutic molecules and release them in response to specific stimuli such as pH,[13–15] temperature,[16,17] redox,[18–22] light,[23,24] and enzyme activity.[25,26]

Nanogels are generally prepared by microemulsion or inverse microemulsion methods. However, these conventional methods are relatively complex and require multiple purification steps to remove unreacted monomers and the surfactants used as emulsion stabilizers. Moreover, these methods have drawbacks, such as limited types of internal payload. On the other hand, the formation of nanogels from linear polymers by intra- and inter-chain collapse can afford a facile protocol toward well-defined delivery vehicles. This method also often requires very dilute conditions and thus potentially limits encapsulation efficiency.

Hyperbranched polyglycerols (PGs) are among the most widely used hyperbranched polymers, and possess a globular polymeric structure comprised of a polyether backbone with a large number of hydroxyl groups.

Reproduced in part with permission from Park, H.; Choi, Y.; Jeena, M.T.; Ahn, E.; Choi, Y.; Kang, M.G.; Rhee, H.W.; Ryu, J.H.; Kim, B.S. unpublished results. Submission for Macromol.Bio.

PGs are actively investigated as an alternative to conventional poly(ethylene glycol), the most biocompatible synthetic polymer, in broad applications such as surfactants, cosmetics, and pharmaceutics owing to their excellent biocompatibility, immunogenicity, and oxidation stability.[27–30] Moreover, recent advances in the development of functional epoxide monomers have expanded the toolkit for the synthesis of functional hyperbranched PGs with responsive properties under specific biological cues. For example, a glycerol monomer containing a disulfide bond, i.e., 2-((2-(oxiran-2-ylmethoxy) ethyl)disulfanyl)ethan-1-ol (SSG), was recently developed by our group to synthesize redox-degradable hyperbranched PGs (PSSGs).[31,32] These PSSGs can offer new opportunities in smart drug delivery systems by taking advantage of considerable redox concentration gradients between intracellular and extracellular environments. Even with these developments, the loading of active therapeutics for redox-responsive PSSGs was limited because of the intrinsic hydrophilicity of hyperbranched PSSGs.

Thus, in continuation of our endeavors in the development of hyperbranched PGs for biomedical applications, we herein demonstrate the synthesis of redox-responsive nanogels from hyperbranched PSSGs that can encapsulate a variety of internal payloads such as hydrophobic/hydrophilic drugs and enzymes. Specifically, we exploited the self-cross-linking chemistry of thiol and disulfide groups within polymeric structures after the addition of a deficient amount of dithiothreitol (DTT) (Figure 1). By varying many synthetic parameters including the fraction of degradable monomers within the polymers (homo- and copolymers), molecular weights, and the degradation degree according to equivalents of a disulfide cleavage agent, we tailored the size and mesh density of the nanogels, which in turn controlled the release profiles of their internal payloads. The nanogel formation employed in the present study circumvents the aforementioned synthetic challenges, generating water-soluble nanogels with high encapsulation capabilities of various active therapeutics and biocompatibility while retaining the responsive behavior for smart drug delivery.

2. Experimental section

2.1. Materials. All reagents and solvents were purchased from Sigma-Aldrich and Acros and used as received unless otherwise stated. Chloroform-d_1 and deuterium oxide were purchased from Cambridge Isotope Laboratory. Doxorubicin hydrochloride (Dox·HCl) was purchased from EP (France). The X-gal assay kit was purchased from BioVision, Inc, USA.

2.2. Measurements. ^{1}H NMR spectra were acquired using a VNMRS 600 spectrometer operating at 400 MHz using D_2O solvents. The number- (M_n) and weight-averaged molecular weights (M_w) and molecular-weight distribution (M_w/M_n) were measured using gel permeation chromatography (GPC, Agilent Technologies 1200 series, USA) with a polystyrene (PS) standard and 0.01 M lithium bromide containing dimethylformamide (DMF) as an eluent at 40 °C with a flow rate of 1.00 mL/min. The morphology and the size of the nanogels were investigated using transmission electron microscopy (TEM, JEM-2100, JEOL, Japan) and atomic force microscopy (AFM, Dimension 3100, Veeco, USA). Hydrodynamic diameter (D_h) was studied using dynamic light scattering (DLS, Nano ZS, Malvern, U.K., and BI-APD, Brookhaven Instrument, New York, USA). Three instruments were used to cross-check the reliability of the obtained data. A UV/vis spectrophotometer (UV-2550, Shimadzu, Japan) was used to measure the absorbance of nanogels containing Nile red. A spectrofluorimeter (RF-6000, Shimadzu, Japan) was also used to obtain the release profiles of dyes from nanogels and to determine the amount of encapsulated FITC-β-gal within nanogels. The calibration curve of doxorubicin (Dox) was obtained by high-performance liquid chromatography (HPLC, Agilent Technologies 1200 series, USA) with a mobile phase of a mixture of CH_3CN and H_2O (6:4, v/v) at a rate of 0.80 mL/min and 20 °C. The detection of Dox was performed by using a UV detector at a wavelength of 480 nm. The fluorescent images were obtained by confocal laser scanning microscopy (CLSM, LSM880, LSM 780, Carl Zeiss, Germany). The X-gal activity assay was carried out with an OLYMPUS Inverted Fluorescence Microscope.

2.3. Synthesis of 2-{2-[2-(Oxiran-2-Ylmethoxy)Ethyl]Disulfanyl}Ethanol (SSG Monomer), (PSSG Homopolymer) and (P(G-*co*-SSG) Copolymer). The SSG monomer and polymer were prepared according to the previously reported method.[31] The M_n of $PSSG_{11}$ (polymer 1) was determined to be 2450 g/mol, as calculated from the NMR data, using the following equation: number of repeating units (n) = 14 (integration value) × 3 (number of

protons in trimethylolpropane (TMP) (methyl, 3H)) / 4 (number of protons neighboring the disulfide moiety of SSG (4H)) = 11; M_n = 210.31 (molecular weight of the SSG monomer) × 11 + 134.17 (molecular weight of the TMP initiator) = 2447.58 g/mol. The M_n of P(G_{21}-*co*-SSG_{13}) (polymer 4) was also determined to be 4420 g/mol, as calculated from the NMR data, using the following equation: number of repeating units (SSG) = 17.47 (integration value) × 3 (number of protons of TMP (methyl, 3H)) / 4 (number of protons neighboring the disulfide moiety of SSG (4H)) = 13, number of repeating units (G) = [75.52 (integration value) × 3 (number of protons of TMP (methyl, 3H)) − {(13 (number of SSG repeating units) × 9 (number of protons of SSG except those that neighbor the disulfide moiety (9H))) − 6 (number of protons of TMP (ether, 6H))}] / 5 (number of protons of the G monomer (5H)) = 21; M_n = 74.08 (molecular weight of the G monomer) × 21 + 210.31 (molecular weight of the SSG monomer) × 13 + 134.17 (molecular weight of TMP) = 4423.88 g/mol (see Table 1 for a summary of all the polymers prepared).

2.4. In situ Formation of Redox Sensitive Nanogels. 50 mg of P(G_{10}-*co*-SSG_{12}) polymer (polymer 3) was dissolved in 1.0 mL deionized water and placed in a flask pre-heated at 70 °C for 10 min. A pre-determined amount of DTT (0.2 and 1.0 mg) that corresponded to 10 and 50 mol % of DTT relative to the disulfide moieties, respectively, was added to the polymer solution and stirred at room temperature for 15 h to allow for degradation and subsequent inter- and intra-molecular cross-linking. The resulting nanogels were purified by dialysis (MWCO 6000 Da, SpectraPore, USA) for 3 days to eliminate any byproducts and residual DTT.

2.5. Nanogels Encapsulated with Hydrophobic Nile Red. 50 mg of P(G_{10}-*co*-SSG_{12}) polymer (polymer 3) and excess Nile red (2 mg) were dissolved in 200 μL of acetone and a measured amount of DTT (0, 0.2, and 1.0 mg, which corresponded to 0, 10, and 50 mol % of DTT relative to the disulfide moieties) was added. After stirring for 10 min, 1.0 mL of deionized water was added, and the mixture was stirred overnight at room temperature while open to the atmosphere, allowing the organic solvent to evaporate. Insoluble excess Nile red was removed by filtration, and the nanogel suspension was dialyzed as described above.

2.6. Release of Encapsulated Nile Red from Nanogel. A 1.0 mL sample of nanogel with encapsulated Nile red was placed inside a dialysis membrane (MWCO 500–1000 Da,

SpectraPore, USA) for 72 h. The fluorescence intensity of the nanogel was determined using a spectrofluorometer at an excitation wavelength of 480 nm with a constant time interval during the release of Nile red through dialysis.

2.7. Nanogel Encapsulated with Dox. 50 mg of P(G_{10}-*co*-SSG_{12}) polymer (polymer 3) was dissolved in 5.0 mL of deionized water and DTT (0, 0.2, and 1.0 mg, which corresponded to 0, 10, 50 mol % of DTT relative to the disulfide moieties, respectively,) was added to the solution. Afterwards, Dox from Dox·HCl (7.5 mg, 0.013 mmol) pretreated with 50% NaOH solution was added slowly into the solution. The pH was adjusted to 7.4 with a phosphate buffer solution (solution mixture of 10 mM KH_2PO_4 and K_2HPO_4). The mixture was stirred for 24 h at room temperature and dialyzed against PBS buffer (pH 7.4) using a dialysis membrane (MWCO 6000 Da, SpectraPore, USA) for 3 days at room temperature while water was changed every day.

2.8. *In Vitro* Cell Cytotoxicity. The cytotoxicity and efficacy of the nanogels in drug delivery were assessed by MTT assays. Briefly, HeLa cells (human epithelial carcinoma cells) and WI-38 cell (human diploid cells) purchased from the Korea Cell Line Bank (Korea) grew in 96-well plate containing Dulbecco's modified Eagle's medium (DMEM), 10% fatal bovine serum (FBS), and 1% penicillin-streptomycin at a density of 3×10^4 cells per well. After stabilizing, the HeLa and WI-38 cells were treated with each nanogel solution and incubated for 24 h at 37 °C in a humidified atmosphere of 95% air/5% CO_2. Thiazolyl blue tetrazolium bromide (MTT, Sigma-Aldrich) was added in each well (final conc. of 0.50 mg/mL) and incubated for 3 h. After removing the culture medium, 100 μL of DMSO was added to each cell well to dissolve the MTT reagent, and the plates were gently agitated for 15 min at room temperature. The absorbance was measured at a wavelength of 540 nm using 620 nm as a reference.

2.9. Cellular Uptake of Nanogels. Cellular uptake of Dox-loaded nanogels and pure nanogels was measured with confocal laser fluorescence microscopy imaging using HeLa cells. HeLa cells were plated on microscope slides in an 8-well tissue culture plate at a density of 3×10^4 cells per well and incubated with DMEM containing 10% FBS and 1% penicillin-streptomycin for 24 h. After pre-incubating, the Dox-loaded nanogels were dissolved in the culture medium to a concentration of 0.50 mg/mL for an additional 6 and 24 h. After washing with PBS (pH

7.4), a solution of 4',6-diamidino-2-phenylindole (DAPI, Sigma-Aldrich; 20 mg/mL in MEM media) was incubated at 37 °C. The cells were fixed with 4% formaldehyde at room temperature after 30 min incubation. Confocal laser scanning microscopy (CLSM) images were taken using a Carl Zeiss LSM880 confocal microscope.

2.10. Preparation of FITC-β-Galactosidase and Dox-loaded Nanogels. 50 mg of P(G_{10}-*co*-SSG_{12}) polymer (polymer 3) was dissolved in 1.0 mL of deionized water and DTT (1.0 mg, which corresponded to 50 mol % of DTT relative to the disulfide moieties, respectively) was added in the solution. Afterwards, Dox (2 mg, 3.7 μmol) and fluorescein isothiocyanate isomer I (FITC)-labeled β-galactosidase (FITC-β-gal, conc. 0.20 mg/mL) were added slowly into the solution. FITC labeling of the β-galactosidase was performed according to the previously reported procedure.[41] The mixture was kept stirring for 24 h at room temperature and dialyzed against PBS buffer using a dialysis membrane (MWCO 6000 Da, SpectraPore, USA) for 3 days at room temperature while water was changed every day. The obtained product was centrifuged to separate the un-encapsulated free β-gal for 10 min at 4000 rpm.

2.11. Confocal Analysis of FITC-labeled β-Galactosidase-loaded Nanogels. The cellular internalization of FITC-labeled β-gal-loaded NGs and intracellular release were monitored with confocal microscopic analysis. The HeLa cells were seeded in 8-well tissue culture plates at a density of 3×10^3 cells per well. After 24 h, the culture medium was exchanged with fresh medium and further treated with NGs loaded with both Dox and FITC-β-gal at a concentration of 1.0 mg/mL for 6 h at 37 °C under 5% CO_2. Confocal laser scanning microscopy (CLSM) images were taken using an Olympus LSM-780 confocal microscope.

2.12. Activity Assay of β-Galactosidase Loaded in Nanogels (X-gal Staining). HeLa cells were seeded in a 12-well tissue culturing plate at 5×10^4 cells/well supplemented with DMEM medium containing 10% FBS and 1% penicillin-streptomycin. After 24 h, the culture medium was removed and exchanged with fresh media containing both Dox and FITC-β-gal-loaded NG4 at a concentration of 1.0 mg/mL. After 24 h, the cells were washed with PBS and X-gal staining was carried out according to the manufacturer's instructions (BioVision, USA). Briefly, cells were fixed with the fixative for 15 min followed by washing with PBS twice, then supplemented with staining materials (470 μL of staining solution, 5 μL of staining supplement,

25 μL of 20 mg/mL of X-gal in DMF), and kept overnight at 37 °C in a non-CO_2 incubator. After 12 h, cells were washed with PBS and imaged with an OLYMPUS inverted fluorescence microscope.

3. Results and Discussion

3.1. Synthesis and characterizations of polymer and nanogel

To provide redox-degradable hyperbranched polyglycerols, we first prepared the SSG monomer as reported previously.[31,32] After synthesis of the SSG monomer, we performed the polymerization to PSSG homopolymers and P(G-*co*-SSG) copolymers via anionic ring-opening multibranching polymerization methods. Five different hyperbranched polymers (both homo- and copolymers) of varying molecular weights ranging from 2240 to 10890 g/mol were successfully prepared, as determined by ^{1}H NMR and GPC analyses (Table 1). We found relatively good agreement between the targeted and calculated molecular weights of polymers that were controlled by the monomer-to-initiator ratio, albeit with noticeable differences in their respective reactivities during polymerization (see Experimental Section for detailed calculations and Figure S1 for ^{1}H NMR spectra). GPC analysis also allowed the characterization of the controlled polymerization of homopolymers and copolymers in a relatively narrow molecular weight distribution (M_w/M_n < 1.5). In addition, all polymers prepared were highly soluble in water and organic polar solvents such as methanol, DMF, and DMSO.

Unlike other studies that described treatment with excess DTT to cleave all redox-degradable moieties, we hypothesized that the addition of an insufficient amount of DTT would cause the cleavage of a well-defined fraction of disulfide groups from the corresponding thiol functionalities. These thiol functionalities would then react with other free thiols either in the same polymer or in neighboring chains to form new disulfide bonds or with other existing disulfide groups in thiol–disulfide exchange chemistry. It is well known that these reactions occur reversibly at room temperature in water without the need for additional catalysts and chemicals.[33] Thus, a series of these reactions eventually results in cross-links within the polymeric aggregates, leading to the formation of nanogels, as shown in Figure 1. As notable examples, Thayumanavan and co-workers have employed the self-cross-linking chemistry of disulfide groups for the formation of various types of nanogels.[10,11,34,35]

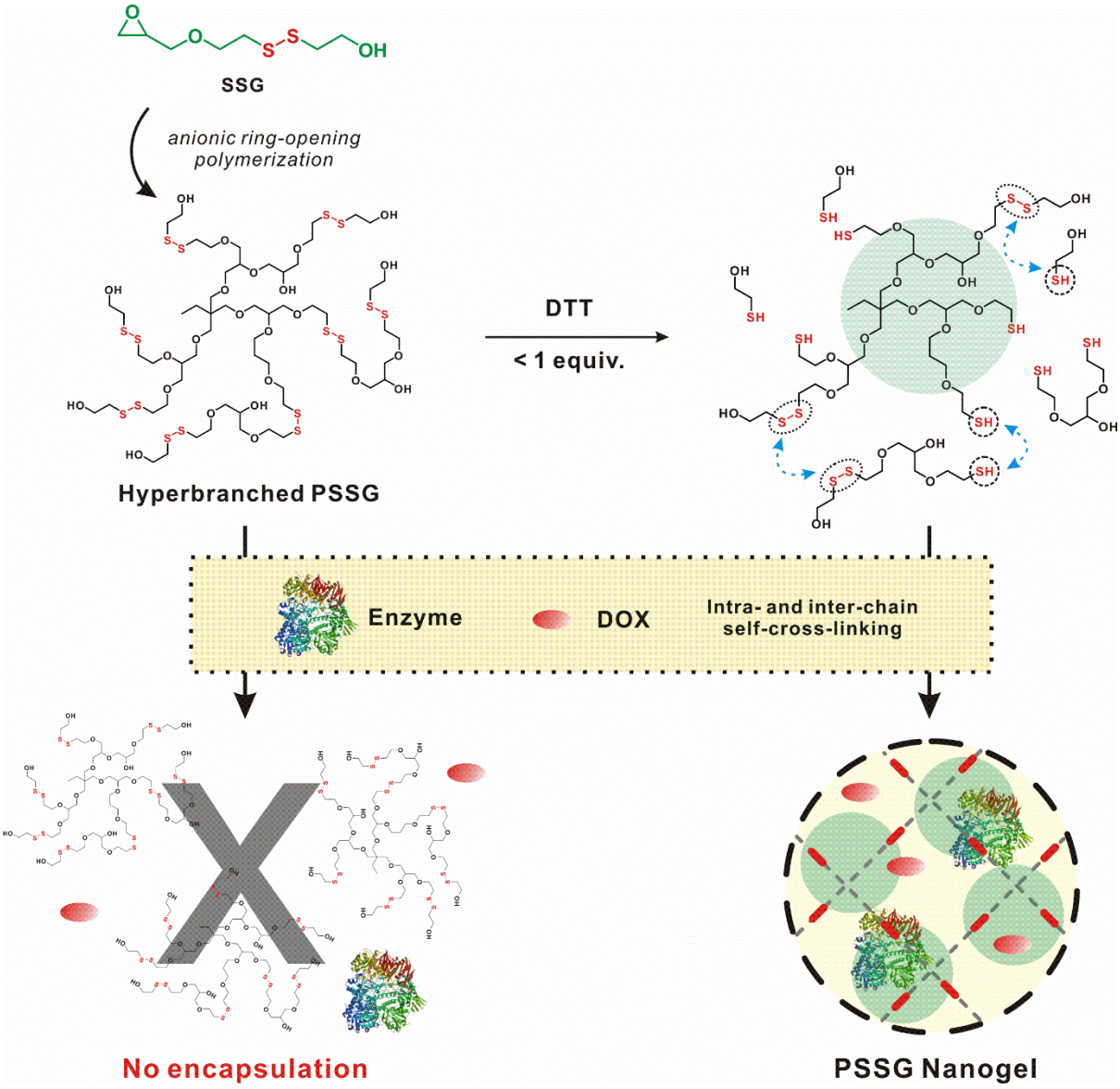

Figure 1. Synthetic scheme for the PSSG polymer and the *in situ* formation of degradable nanogels through thiol–disulfide exchange and disulfide exchange chemistry (marked with blue arrows) between inter- and intra-molecular chains upon treatment with DTT. Other chains are not depicted for clarity. Green circle represents the basic unit for the formation of the PSSG nanogel.

Table 1. Characterization data of polymers used in this study.

No	Polymer composition (target)	Polymer composition (NMR)[a]	M_n (target)	% SSG (target)	M_n (NMR)[a]	% SSG (NMR)[a]	M_n (GPC)[b]	M_w/M_n[b] (GPC)[b]
1	$PSSG_{10}$	$PSSG_{11}$	2240	100	2450	100	3600	1.53
2	$PSSG_{30}$	$PSSG_{30}$	6440	100	6440	100	6300	1.30
3	$P(G_{10}\text{-co-}SSG_{20})$	$P(G_{10}\text{-co-}SSG_{12})$	5080	66.7	3400	54.6	4400	1.24
4	$P(G_{20}\text{-co-}SSG_{20})$	$P(G_{21}\text{-co-}SSG_{13})$	5820	50.0	4420	38.2	5000	1.25
5	$P(G_{60}\text{-co-}SSG_{30})$	$P(G_{46}\text{-co-}SSG_{18})$	10890	33.3	7460	28.1	5400	1.38

[a] Determined via ^1H NMR spectroscopy. [b] Measured using GPC-RI in DMF with a polystyrene standard.

3.2. Size controllable NGs with varying amount of DTT

To investigate the effect on the formation of nanogels with different amounts of DTT, we prepared nanogels treated with 10 to 50 mol % of DTT relative to the disulfide moieties within the polymer (Figure 2a). As representative examples, we chose homopolymer $PSSG_{30}$ (polymer 2) and copolymer P(G_{10}-*co*-SSG_{12}) (polymer 3) for the formation of nanogels and denoted their respective nanogels with varying amounts of DTT as NG*n* (see Table 2 for the notation of NGs).

As clearly observed in the atomic force microscopy (AFM) images of the NGs in Figure 2b, both polymers successfully formed NGs after treatment with defined amounts of DTT. Interestingly, the controlled sizes of cross-linked NGs were shown with average diameters of 142 ± 30 and 78 ± 8.3 nm for NGs prepared from $PSSG_{30}$ homopolymer, and 178 ± 54 and 74 ± 12 nm for P(G_{10}-*co*-SSG_{12}) copolymer with 10 and 50 mol % DTT treatment, respectively (Table 2). This observation can be explained on the basis of the balance between the degradation of the polymer into smaller fragments and subsequent reassembly into cross-linked NGs. Specifically, it suggests that the NGs prepared by treatment with a smaller amount of DTT (i.e., 10 mol %) were less cross-linked because smaller quantities of free thiols were allowed to react with disulfide groups or thiol groups in other chains, eventually leading to large, yet loosely cross-linked NGs. Transmission electron microscopy (TEM) micrographs further supported that these NGs possessed a spherical morphology with a particle size in accordance with the AFM results. In parallel, DLS studies indicated that the hydrodynamic diameters (D_h) of NGs obtained from P(G_{10}-*co*-SSG_{12}) copolymers treated with various concentrations of DTT were significantly changed from the pristine polymers (Figure 3). For example, the D_h of NGs prepared by treatment with 10, 20, and 50 mol % DTT were 249 ± 71, 203 ± 52, and 79 ± 21 nm, respectively. Interestingly, the D_h of pristine P(G_{10}-*co*-SSG_{12}) copolymer itself indicated a D_h of only 2 nm, clearly demonstrating the absence of self-aggregation of the initial polymers without the introduction of reducing chemicals. The average D_h values (obtained using DLS) of the NGs were slightly larger than those observed by AFM and TEM, which can be attributed to the swelling of the NGs in water (Table 2). We also monitored the size tunability of NGs upon changes in the concentration of the initial polymer solution; for example, when the concentration was doubled to 100 mg/mL, the D_h of NG4 increased considerably from 79 ± 21 nm to 585 ± 102 nm.

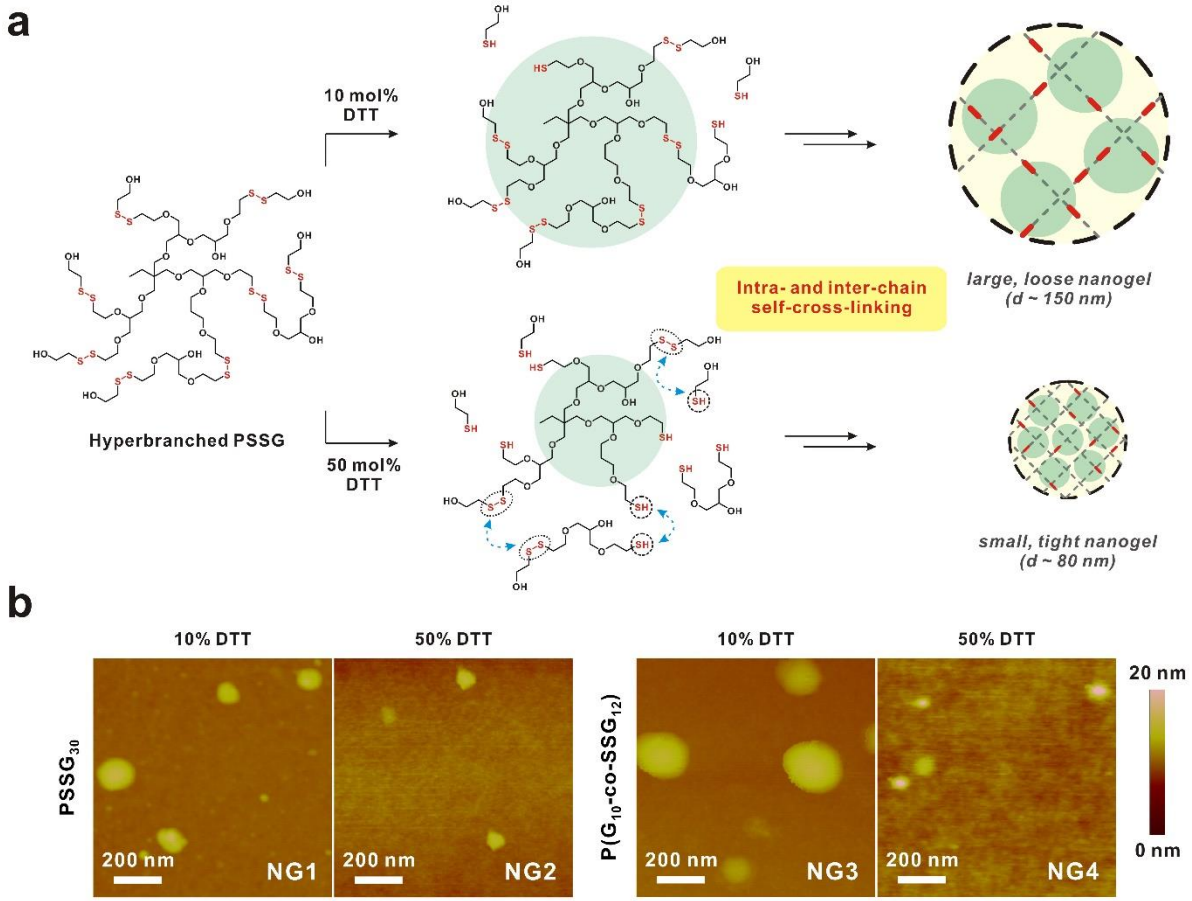

Figure 2. (a) Scheme for the synthesis of size-controllable PSSG nanogels with different amounts of DTT. (b) Representative AFM images of nanogels (NGs) prepared from $PSSG_{30}$ homopolymer (polymer 2) and $P(G_{10}$-*co*-$SSG_{12})$ copolymer (polymer 3) with 10 and 50 mol % of DTT.

Table 2. Characterization data of nanogels prepared in this study.

Nanogel	Polymer[a]	DTT (mol%)	AFM (nm)	TEM (nm)	DLS (nm)
NG1	$PSSG_{30}$	10	142 ± 30	194 ± 34	220 ± 52
NG2	$PSSG_{30}$	50	78 ± 8.3	57 ± 6.7	85 ± 14
NG3	$P(G_{10}$-*co*-$SSG_{12})$	10	178 ± 54	168 ± 42	249 ± 71
NG4	$P(G_{10}$-*co*-$SSG_{12})$	50	74 ± 12	80 ± 16	79 ± 21

[a] Concentration of all polymers is 50 mg/mL.

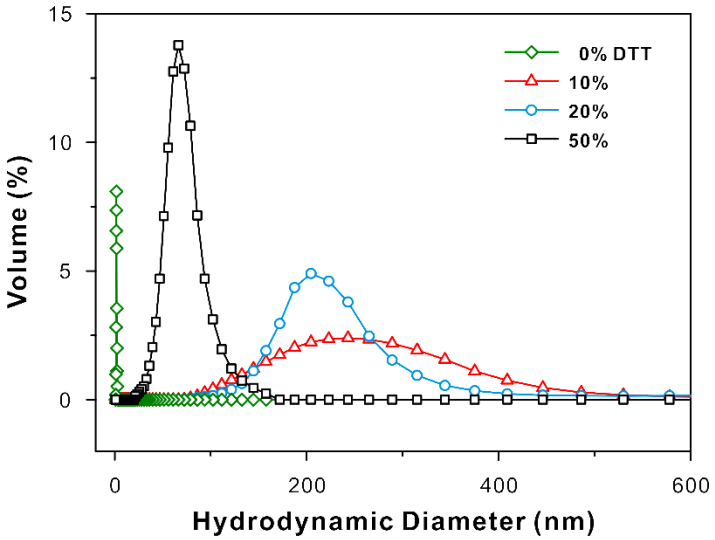

Figure 3. Hydrodynamic diameter (D_h) of NGs prepared from P(G_{10}-*co*-SSG_{12}) copolymer (polymer 3) with varying degrees of DTT treatment. Note that the D_h of the initial P(G_{10}-*co*-SSG_{12}) copolymer (green) is determined to be only 2 nm.

3.3. Release kinetics of therapeutics from NGs

To investigate the stability of the NGs, we characterized the encapsulation efficiency using the hydrophobic Nile red stain as a model therapeutic payload. Because of the limited aqueous solubility of Nile red, we used acetone as a co-solvent during the formation of the NGs and simultaneous loading of Nile red. The relative encapsulation efficiency of Nile red is considerably different between the NGs. For example, NG2 retained a significantly higher loading of approximately 8 times than that of NG1, albeit with smaller dimensions, as determined by AFM and DLS. Similarly, NG4 displayed a 12 times higher loading capacity of Nile red per unit volume than NG3. Thus, loading capacity depends on cross-linking density. This result again highlights the high tunability of our NGs in terms of loading capacity with the facile treatment of a reducing chemical reagent. Furthermore, we investigated the release of Nile red encapsulated within NGs. As shown in Figure 4, large and loosely cross-linked NG1 and NG3 both demonstrated more rapid release, while small and densely cross-linked NG2 and NG4 displayed a slower release over time. This observation clearly suggests that the cross-linking density is responsible for controlling the rate of payload release from the NGs. Another interesting feature of the redox-responsive NG system is that it can further release the internal payload in response to additional reducing stimuli. Because the NGs are still cross-linked by disulfide bonds, Nile red can be further released upon treatment with DTT as an active delivery mode. As such, when we introduced additional DTT at a designated time point, we could observe the enhanced release kinetics. For example, the relative release percentages of Nile red from NG1 and NG2 for 12 h are 43% and 32%, respectively, in the case of passive release. On the other hand, the relative release percentages from NG1 and NG2 are 82% and 84%, respectively, in the active release mode. Consequently, the addition of DTT to stable NGs containing active therapeutic agents can facilitate more rapid release than that of the NGs alone. Taken together, we argue that redox-degradable NGs can be beneficial in achieving active therapeutic delivery with a wide range of tunability in their size and controllable release kinetics, which can potentially be applied in response to the higher reducing environments inside the cytoplasm.

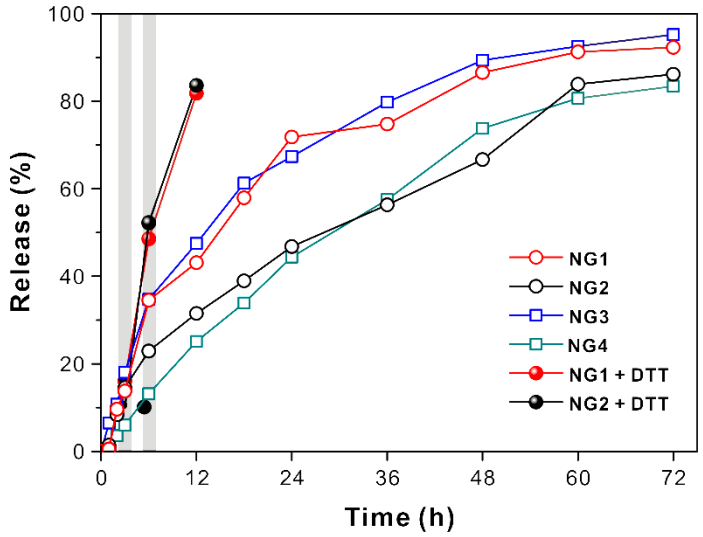

Figure 4. Release profile of Nile red from NGs with different cross-linking densities. Note that the shaded time points represent treatment of the Nile red-loaded NGs with additional DTT for an active delivery mode.

3.4. *In vitro* cell viability and CLSM images

Encouraged by the successful synthesis and control over the release kinetics of the model therapeutic from the nanogels, we evaluated their cytotoxicity to investigate their potential in biomedical settings. The *in vitro* cytotoxicity of each NG was assessed via the MTT assay using WI-38 (human diploid cells) and HeLa (human epithelial carcinoma cells) cell lines as models of normal and cancer cells, respectively. The cell viability of each cell line treated with the polymeric nanogels was greater than 80%, even up to a concentration of 1000 μg/mL, which is beyond the common concentration ranges usually tested. These results indicate that all NGs are highly biocompatible and non-toxic to both cell lines. Moreover, *in vitro* efficacy for the intracellular delivery of the active therapeutic agent from Dox-loaded NGs was investigated by a cell viability assay using a human cervical cancer HeLa cell line. As shown in Figure 5a, the Dox-loaded NG4 nanogels induced significant cytotoxicity in HeLa cells, while virtually no toxicity was observed from NG4 over the entire concentration range tested. The concentration at which the cell viability decreased to 50% using Dox/NG4 was estimated to be approximately 0.04 μM of Dox as determined from HPLC. This value is found to be higher than the reported IC_{50} of Dox (~0.015 μM).[36] The cellular uptake efficiency of Dox-loaded NG4 was further studied by confocal laser scanning microscopy (CLSM) (Figure 5b). The encapsulated Dox was slowly released when the Dox-loaded NG4 was delivered at the cell cytoplasm, which spread to all parts of the cytoplasm within 6 h. After 24 h, it was found inside the nucleus and several pores were generated by cellular apoptosis induced by the effective delivery of Dox. It was observed that the Dox-loaded NG4 was located within the endosomal vesicles, releasing Dox in a controlled manner.

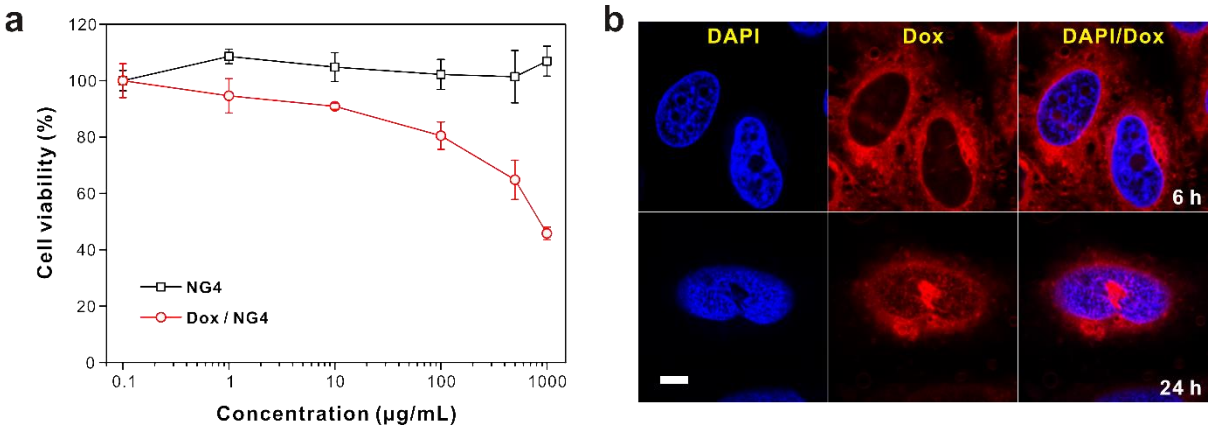

Figure 5. (a) *In vitro* cell viability assay of plain NG4 (black) and Dox-loaded NG4 (red). (b) CLSM images of HeLa cells incubated with Dox-loaded NG4 for 6 h (top panel) and 24 h (bottom panel). Each channel corresponds to the fluorescence of DAPI for cell nucleus and Dox for drug delivery. Scale bar is 20 μm.

3.5. Co-delivery efficacy of the drug loaded NGs *in vitro*

Combination therapies are of special interest and provide a high potential for increased efficacy through synergistic interplay between therapeutics.[37-40] Simultaneous delivery of proteins and small molecular drugs is a compelling strategy that has been employed in cancer therapy and immunotherapy.[41] One key challenge in the co-delivery of active therapeutic agents is the distinct physicochemical properties required for each component, particularly for hydrophobic and hydrophilic components, such as in the delivery of hydrophobic small molecules along with large hydrophilic proteins. We hypothesize in this study that concurrent delivery of enzyme and active drug is indeed feasible with redox-responsive NGs. As a proof-of-concept, we employed the β-galactosidase functionalized with fluorescein (FITC-β-gal) as a hydrophilic protein and Dox as a hydrophobic small therapeutic encapsulated within the NG4 (see the Experimental section for details). When the NG4 dual-loaded with Dox and FITC-β-gal was incubated with HeLa cells for 12 h, Dox was transported into the cytosol and nucleus, while FITC-β-gal existed in the lysosome as shown in Figure 6a. As the NGs consist of bioreducible disulfide bonds, the release of the encapsulated protein and small molecule can be triggered upon exposure to glutathione (GSH), a biological cue present at higher concentration inside cells than in the extracellular environment. The co-localization of both Dox and FITC-β-gal was successfully confirmed by the overlay of each fluorescence color in the merged image, suggesting the effective intracellular delivery of NGs regardless of the size and types of payload. Based on the fluorescence intensity measurement, the amount of loaded FITC-β-gal was determined to be about 8.6 μg/mL at a concentration of 50 mg/mL of NG4. In addition, the D_h of NG4 loaded with both FITC-β-gal and Dox is larger than pure NG4 and NG4 loaded with only FITC-β-gal. Finally, we demonstrated that the protein activity is retained after internalization into the cells using the X-gal activity assay (Figure 6b). The HeLa cells incubated with NG4 loaded with β-gal exhibited a dark blue color because of the conversion of the 5-bromo-3-indoyl-β-$_D$-galactopyranoside into a corresponding indigo derivative by β-gal. In contrast, the control experiment revealed a weak blue color scattered inside the cells because of the presence of internal β-gal in the lysosome. Moreover, considering that the cellular membrane is not permeable to β-gal itself and that the hydrophobic dye is not soluble in water, these results confirmed the critical role of NGs in the concurrent delivery of a functional protein and a therapeutic agent inside the cells.

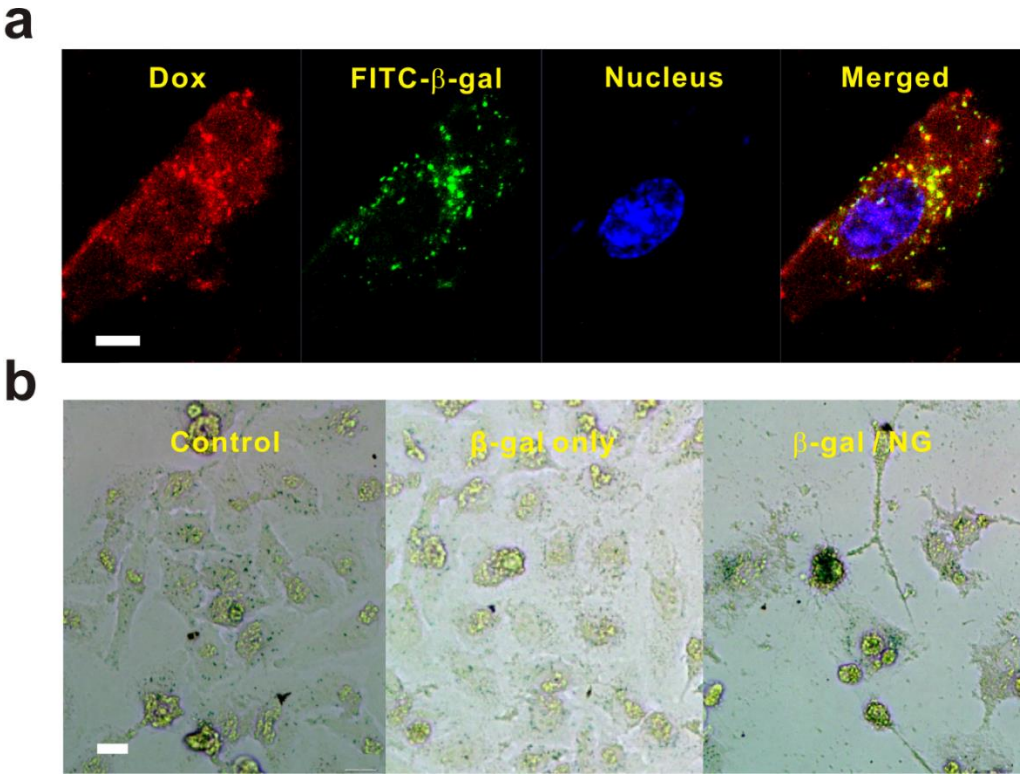

Figure 6. (a) CLSM images of HeLa cells incubated with NG4 loaded with both Dox and the FITC-labeled β-galactosidase (FITC-β-gal). Each channel corresponds to the red color of Dox, the green for FITC-β-gal, and the blue Hoechst stain in the cell nucleus. (b) X-gal activity assay of delivered β-gal into HeLa cells using NG4. Control samples of free cells and β-gal only. Note that the free cells indicate the X-gal activity due to the presence of internal β-gal in the lysosome. Scale bar is 10 μm.

4. Conclusion

In summary, we developed a self-cross-linked hyperbranched polyglycerol nanogel using the thiol–disulfide exchange reaction based on a novel disulfide-containing polymer. The highly tunable nature of the size and cross-linking density of the resulting nanogel was controlled by the type of polymer (homo- or copolymer) and the amount of reducing agent, dithiothreitol, used in the preparation of the nanogels. In situ encapsulation of various therapeutic agents irrespective of hydrophilic and hydrophobic nature and molecular weight was accomplished with the intra- and inter-molecular thiol-disulfide exchange reaction and new disulfide bond formation within hyperbranched polymers. Their superior biocompatibility together with the controllable release of active therapeutic agents that are still functional inside cells show the applicability of nanogels in smart drug delivery systems. We anticipate that redox-responsive nanogels will provide a promising platform to mediate the delivery of a wide range of active therapeutics in a time-specific and stimulus-specific manner.

References

1. Chacko, R. T.; Ventura, J.; Zhuang, J.; Thayumanavan, S. *Adv. Drug Deliv. Rev.* **2012**, *64*, 836–851.

2. Zhang, X.; Malhotra, S.; Molina, M.; Haag, R. *Chem. Soc. Rev.* **2015**, *44*, 1948–1973.

3. Wu, H. Q.; Wang, C. C. *Langmuir* **2016**, *32*, 6211–6225.

4. Oh, J. K.; Drumright, R.; Siegwart, D. J.; Matyjaszewski, K. *Prog. Polym. Sci.* **2008**, *33*, 448–477.

5. Sisson, A. L.; Haag, R. *Soft Matter* **2010**, *6*, 4968–4975.

6. An, Z.; Qiu, Q.; Liu, G. *Chem. Commun.* **2011**, *47*, 12424–12440.

7. Fleige, E.; Quadir, M. A.; Haag, R. *Adv. Drug Deliv. Rev.* **2012**, *64*, 866–884.

8. An, S. Y.; Arunbabu, D.; Noh, S. M.; Song, Y. K.; Oh, J. K. *Chem. Commun.* **2015**, *51*, 13058–13070.

9. Steinhilber, B. D.; Sisson, A. L.; Mangoldt, D.; Welker, P.; Licha, K.; Haag, R. *Adv. Funct. Mater.* **2010**, *20*, 4133–4138.

10. Ryu, J. H.; Jiwpanich, S.; Chacko, R.; Bickerton, S.; Thayumanavan, S. *J. Am. Chem. Soc.* **2010**, *132*, 8246–8247.

11. Ryu, J. H.; Bickerton, S.; Zhuang, J.; Thayumanavan, S. *Biomacromolecules* **2012**, *13*, 1515–1522.

12. Cao, Z.; Zhou, X.; Wang, G. *ACS Appl. Mater. Interfaces* **2016**, *8*, 28888–28896.

13. Morimoto, N.; Hirano, S.; Takahashi, H.; Loethen, S.; Thompson, D. H.; Akiyoshi, K. *Biomacromolecules* **2013**, *14*, 56–63.

14. Molla, M. R.; Marcinko, T.; Prasad, P.; Deming, D.; Garman, S. C.; Thayumanavan, S. *Biomacromolecules* **2014**, *15*, 4046–4053.

15. Liu, B.; Thayumanavan, S. *J. Am. Chem. Soc.* **2017**, *139*, 2306–2317.

16. Moon, H. J.; Ko, D. Y.; Park, M. H.; Kyung, J. M.; Jeong, B. M. *Chem. Soc. Rev.* **2012**, *41*, 4860–4883.

17. Sun, J.; Yu, Z.; Hong, C.; Pan, C. *Macromol. Rapid Commun.* **2012**, *33*, 811–818.

18. Liu, J.; Pang, Y.; Huang, W.; Zhu, Z.; Zhu, X.; Zhou, Y.; Yan, D. *Biomacromolecules* **2011**, *12*, 2407–2415.

19. Chen, W.; Zheng, M.; Meng, F.; Cheng, R.; Deng, C.; Feijen, J.; Zhong, Z. *Biomacromolecules* **2013**, *14*, 1214–1222.

20. Urakami, H.; Hentschel, J.; Seetho, K.; Zeng, H.; Chawla, K.; Guan, Z. *Biomacromolecules* **2013**, *14*, 3682–3688.

21. Singh, S.; Topuz, F.; Hahn, K.; Albrecht, K.; Groll, J. *Angew. Chem. Int. Ed.* **2013**, *52*, 3000–3003.

22. Chan, N.; An, S. Y.; Oh, J. K. *Polym. Chem.* **2014**, *5*, 1637–1649.

23. Nishimura, T.; Takara, M.; Mukai, S.; Sawada, S.; Sasaki, Y.; Akiyoshi, K. *Chem. Commun.* **2015**, *52*, 1222–1225.

24. Panja, S.; Dey, G.; Bharti, R.; Mandal, P.; Mandal, M.; Chattopadhyay, S. *Chem. Mater.* **2016**, *28*, 8598−8610.

25. Wu, Changzhu; Böttcherb, Christoph; Haag, R. *Soft Matter* **2015**, *11*, 972–980.

26. Wu, C.; Strehmel, C.; Achazi, K.; Chiappisi, L.; Dernedde, J.; Lensen, M. C.; Gradzielski, M.; Ansorge-schumacher, M. B.; Haag, R. *Biomacromolecules* **2014**, *15*, 3881–3890.

27. Sisson, A. L.; Steinhilber, D.; Rossow, T.; Welker, P.; Licha, K.; Haag, R. *Angew. Chem. Int. Ed.* **2009**, *48*, 7540–7545.

28. Wilms, D.; Stiriba, S.; Frey, H. *Acc. Chem. Res.* **2010**, *43*, 129–141.

29. Shenoi, R. A.; Lai, B. F. L.; Imran Ul-Haq, M.; Brooks, D. E.; Kizhakkedathu, J. N. *Biomaterials* **2013**, *34*, 6068–6081.

30. Herzberger, J.; Niederer, K.; Pohlit, H.; Seiwert, J.; Worm, M.; Wurm, F. R.; Frey, H. *Chem. Rev.* **2016**, *116*, 2170–2243.

31. Son, S.; Shin, E.; Kim, B. S. *Macromolecules* **2015**, *48*, 600–609.

32. Son, S.; Park, H.; Shin, E.; Shibasaki, Y.; Kim, B. S. *J. Polym. Sci. Part A Polym. Chem.* **2016**, *54*, 1752–1761.

33. Singh, R.; Whitesides, G. M. *Sulfur-Containing Functional Groups;* Patai, S., Eds.; J. Wiley and Sons, Ltd., **1993**.

34. Ryu, J. H.; Roy, R.; Ventura, J.; Thayumanavan, S. *Langmuir* **2010**, *26*, 7086–7092.

35. Ryu, J. H.; Chacko, R. T.; Jiwpanich, S.; Bickerton, S.; Babu, R. P.; Thayumanavan, S. *J. Am. Chem. Soc.* **2010**, *132*, 17227–17235.

36. Istomin, Y. P.; Zhavrid, E. A.; Alexandrova, E. N.; Sergeyeva, O. P.; Petrovich, S. V. *Exp. Oncol.* **2008**, *30*, 56–59.

37. Wei, L.; Cai, C.; Lin, J.; Chen, T. *Biomaterials* **2009**, *30*, 2606–2613.

38. Numata, K.; Yamazaki, S.; Naga, N. *Biomacromolecules* **2012**, *13*, 1383–1389.

39. Kim, Y.; Kim, C.; Song, S. *ACS Macro Lett.* **2016**, *5*, 297–300.

40. Alex, M. R. A.; Nehate, C.; Veeranarayanan, S.; Kumar, D. S.; Kulshreshtha, R.; Koul, V. *Biomaterials* **2017**, *133*, 94–106.

41. Gonza, D. C.; Ryu, J. H.; Chacko, R. T.; Zhuang, J; Thayumanavan, S. *J. Am. Chem. Soc.* **2012**, *134*, 6964–6967.

Acknowledgements

어느덧 KBS group에서 짧지 않은 3년이란 시간이 흘렀습니다. 3년이란 시간동안 여러 일들이 있었고 이를 계기로 제가 한걸음 더 성장할 수 있는 시간들이었던 것 같습니다.

가장 먼저, KBS group에서 석사 과정을 잘 마칠 수 있게 지도해주신 김 병수 교수님께 감사의 인사를 올립니다. 더불어 바쁘신 와중에도 학위 디펜스와 학위 논문을 심사해주신 유 자형 교수님, 권 태혁 교수님께도 감사의 말씀을 전합니다. 그리고 학부 때부터 석사 과정까지 옆에서 힘이 되어주었던 KBS group 연구실 멤버들, 최 유리 박사님, 개그맨 응진오빠, 축구왕 민수오빠, 치킨왕 이슬언니, 스마일왕 민주언니, 고생하고 있는 랩장 준희오빠, 나의 든든한 4명의 동기들, 키다리아저씨 영규오빠, 스페셜한 균혁오빠, 리액션왕 송아언니, 유일한 동갑 재은이 그리고 아직 파릇파릇한 1년차 후배들 태형이, 민성이, 윤경이, 은별이 모두에게 감사의 인사 올립니다.

또한, 먼 타지에서 오랜 기간 잘 적응 할 수 있게 서로 의지해온 내 사랑 여신팸 (충연, 수연, 영수, 윤지, 다영, 유나), 즐겁거나 슬픈 모든 일들을 함께 해준 OT 조 (유진, 영렬, 태윤, 다정, 본영) 친구들, 6년째 함께 해온 우리 야시장팸 (종현, 진우, 민우, 영훈, 원주 태경 등등), 그리고 서울 갈 때마다 촌년을 데리고 놀아준 고등학교 내 베프들 (가영, 지은, 하윤, 진희, 현주, 지원) 모두에게 고맙다는 말을 전하고 싶습니다.

마지막으로 가족들에게도 감사의 말씀을 전합니다. 약 6년간 타지 생활하는 동안 부모님을 자주 못 뵙고 딸 노릇을 못했던 것 같은데 앞으로는 애교 많은 맏딸이 되어 효도하겠습니다. 아빠, 엄마! 넘치는 사랑으로 키워 주셔서 감사하고 이 사랑에 보답하겠습니다. 존경합니다. 그리고 중국 유학 중인 동생에게도 하나 뿐인 핏줄로서 항상 응원하고 있고 사랑한다고 전하고 싶습니다.

KBS group에서 배운 지식과 성장 해온 경험들을 바탕으로 사회에 나가서도 의미 있는 일을 할 수 있는 박 해리가 되겠습니다. 모두들 감사합니다!